APPLIED SCIENCES AND ENGINEERING

Orally administrated liquid metal agents for inflammation-targeted alleviation of inflammatory bowel diseases

Miaodeng Liu[1,2,3,4]†, Jinhui Zou[2,3,4,5]†, Heli Li[2,3,4,5], Yunfan Zhou[2,3,4,5], Qiying Lv[2,3,4], Qian Cheng[1,2,3,4], Jia Liu[2,3,4], Lin Wang[1,2,3,4]*, Zheng Wang[2,3,4,5]*

Rapid drug clearance and off-target effects of therapeutic drugs can induce low bioavailability and systemic side effects and gravely restrict the therapeutic effects of inflammatory bowel diseases (IBDs). Here, we propose an amplifying targeting strategy based on orally administered gallium (Ga)-based liquid metal (LM) nano-agents to efficiently eliminate reactive oxygen and nitrogen species (RONS) and modulate the dysregulated microbiome for remission of IBDs. Taking advantage of the favorable adhesive activity and coordination ability of polyphenol structure, epigallocatechin gallate (EGCG) is applied to encapsulate LM to construct the formulations (LM-EGCG). After adhering to the inflamed tissue, EGCG not only eliminates RONS but also captures the dissociated Ga to form EGCG-Ga complexes for enhancive accumulation. The detained composites protect the intestinal barrier and modulate gut microbiota for restoring the disordered enteral microenvironment, thereby relieving IBDs. Unexpectedly, LM-EGCG markedly decreases the *Escherichia_Shigella* populations while augmenting the abundance of *Akkermansia* and *Bifidobacterium*, resulting in favorable therapeutic effects against the dextran sulfate sodium-induced colitis.

INTRODUCTION

Gut microbiota dysbiosis, featuring an immoderate proliferation of profitless microbes and a decrease in beneficial bacteria, plays an important role in the progress of multiple diseases, such as inflammatory bowel diseases (IBDs) and tumors (*1*, *2*). Although conventional therapeutic approaches for IBDs have mainly focused on suppressing hyperactive immune responses in inflamed tissues, a growing body of evidence has indicated that reprograming gut microbiota is highly beneficial to IBD alleviation (*3*–*5*). Accordingly, numerous efforts have been made to develop effective strategies to modulate gut microbiota for IBD alleviation (*6*–*9*). However, IBD treatment remains a challenge since the first-line drugs show side effects and limited therapeutic efficiency due to the complicated etiology and pathogenesis of IBDs (*4*, *10*–*12*). Besides, the neglected overproduced reactive oxygen and nitrogen species (RONS)–induced serious inflammatory response and the poor efficacy of intestinal flora regulation have markedly offset the therapeutic effects of IBDs (*13*, *14*). Therefore, exploiting orally administered agents that can precisely reprogram gut microbiota and synchronously eliminate RONS is of great significance for IBD management.

As an indispensable nutrient for bacterial survival, proliferation, and bacterial infection, iron is involved in many vital metabolic processes, including energy generation and DNA synthesis (*15*–*17*). Biological systems of bacteria are unable to distinguish gallium from iron ions due to their analogous structural features and physicochemical properties (*18*, *19*). As a result, bacteria would specifically take in Ga^{3+} through iron ion uptake pathways in the absence of iron. Of note, Ga^{3+} cannot be reduced under physiological conditions, making Ga^{3+} a potential "tool" for bacterial regulation (*18*, *20*–*22*). Correspondingly, gallium-based compounds have been applied to inhibit pathogenic bacteria without causing bacterial resistance (*23*–*25*). For instance, ultrasmall nonantibiotic gallium-indocyanine green nanoparticles were applied to eradicate biofilms and against drug-resistant bacterial liver abscesses (*26*). Therefore, designing nano-agents for delivering Ga^{3+} to infection sites would be a promising strategy for bacterial modulation.

Gallium (Ga)-based liquid metal (LM), characterized by favorable plasticity and excellent biocompatibility (*27*, *28*), has received increasing attention in stretchable electronic devices, microfluidic systems, and biomedical applications (*29*–*31*). The extraordinary photothermal conversion efficiency, large specific surface area, and special metallic surface properties of LM have rendered LM-based formulations as excellent candidates for drug delivery platforms and photothermal agents in cancer therapy (*32*–*36*). Recently, gallium-based LMs have attracted tremendous interest as potential anti-infection agents for their satisfactory bacterial-modulation performance (*37*–*39*). For example, an LM-based soil system can enrich the gut bacterial diversity and rectify bacterial dysbiosis under a pathophysiological condition (*40*), and gallium-based LMs have been applied to construct acid-responsive micromotors against the *Helicobacter pylori*–caused infections (*41*). Nevertheless, despite a few inspiring applications, gallium-based LM in cancer therapy or bacterial regulation is still at its preliminary stage.

Epigallocatechin gallate (EGCG), a major bioactive polyphenol in green tea (*42*), can not only coordinate with metal ions but also adhere to the biomolecules owing to its polyphenolic hydroxyl structure that has anti-oxidation and strong adhesivity (*43*–*45*). Here, we proposed an EGCG-coated LM nano-agent (LM-EGCG)

[1]Department of Clinical Laboratory, Union Hospital, Tongji Medical College, Huazhong University of Science and Technology, Wuhan 430022, China. [2]Hubei Provincial Engineering Research Center of Clinical Laboratory and Active Health Smart Equipment, Wuhan 430022, China. [3]Research Center for Tissue Engineering and Regenerative Medicine, Union Hospital, Tongji Medical College, Huazhong University of Science and Technology, Wuhan 430022, China. [4]Hubei Key Laboratory of Regenerative Medicine and Multi-disciplinary Translational Research, Wuhan 430022, China. [5]Department of Gastrointestinal Surgery, Union Hospital, Tongji Medical College, Huazhong University of Science and Technology, Wuhan 430022, China.
*Corresponding author. Email: lin_wang@hust.edu.cn (L.W.); zhengwang@hust.edu.cn (Z.W.)
†These authors contributed equally to this work.

to efficiently eliminate RONS and modulate the dysregulated microbiome for remission of IBDs by amplification targeting strategy based on reassembly of Ga^{3+} and EGCG. After LM-EGCG degradation (Fig. 1), the dissociative EGCG could not only adhere to electropositive inflamed tissue to eliminate RONS but also capture dissociated Ga^{3+} to form metal polyphenol complex, thereby improving Ga^{3+} accumulation to modulate gut microbiota. Besides, the impaired intestinal barrier was protected and the overall abundance and diversity of gut microbiota were increased after oral admonition of LM-EGCG, resulting in favorable therapeutic outcomes against the dextran sulfate sodium (DSS)–induced colitis. LM-EGCG markedly decreased pathogenic *Escherichia_Shigella* populations while augmenting the abundance of *Akkermansia* and *Bifidobacterium*, which are crucial microbes in gut homeostasis. This work proposes an amplifying targeting strategy based on the reassembly of EGCG and Ga^{3+} for efficient remission of IBDs, which broadens the horizons of Ga-based LM in biomedical applications.

RESULTS

Construction and characterization of LM-EGCG

Before LM-EGCG synthesis, the performance of Ga^{3+} and organic ligands to form complexes in the intestinal fluid simulation was investigated. Predictably, Ga^{3+} promptly formed complexes at the existence of those of ligands containing polyphenolic hydroxyl structure, especially EGCG, in intestinal fluid simulation (fig. S1). Therefore, we further inquired into the variation of the mixture of EGCG and Ga^{3+} in different conditions. Individual EGCG or Ga^{3+} would not form macroscopic complex precipitation in simulated gastric fluid, simulated intestinal fluid, and simulated colonic fluid (SCF) (Fig. 2A). Because of the complexation of EGCG with Ga^{3+} in alkalescent SCF, the hydrodynamic size of the mixture containing EGCG and Ga^{3+} increased to approximately 2 μm (Fig. 2C) and a great deal of buff floccule appeared in the mixture, which increased with longer placement time (Fig. 2B). Encouraged by the phenomenon that EGCG could capture Ga^{3+} to form complex in SCF, we synthesized the complex of EGCG with Ga (Ga-EGCG) and the EGCG-coated LM nano-agent according to our previous report (*21*). Transmission electron microscopy (TEM) images revealed that the size of LM-EGCG was about 250 nm, and the thickness of EGCG shell was approximately 60 nm (Fig. 2D). Moreover, the relative content of EGCG in LM-EGCG was analyzed using thermogravimetric analyzer (TGA), which revealed that almost a 21% weight decrease occurred in LM-EGCG (Fig. 2E), indicating about 21% loading efficiency of EGCG.

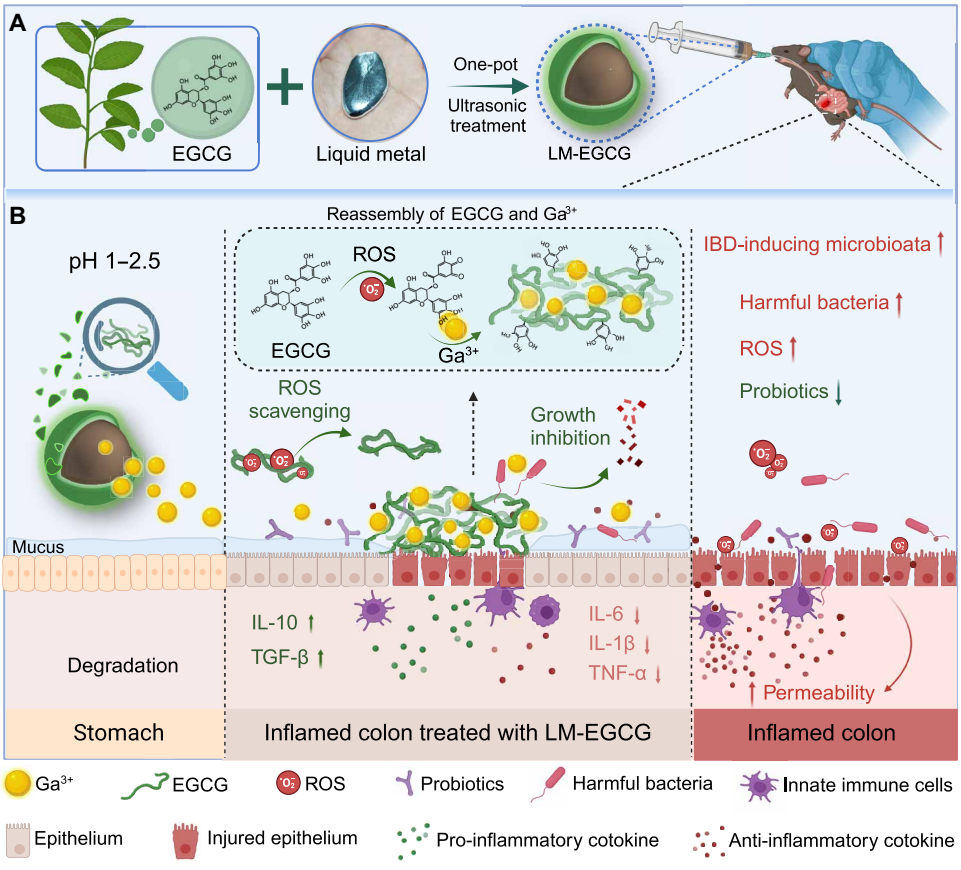

Fig. 1. Schematic illustration of the construction of LM-EGCG and the mechanism for colitis treatment. (**A**) LM-EGCG was successfully constructed by one-pot ultrasonic treatment and orally administered for IBD therapy. (**B**) The process of pH-mediated degradation of LM-EGCG in the stomach and reassembly of EGCG with Ga^{3+}, thereby modulating the dysregulated microbiome, intestinal barrier, and immune responses for alleviating inflammation diseases.

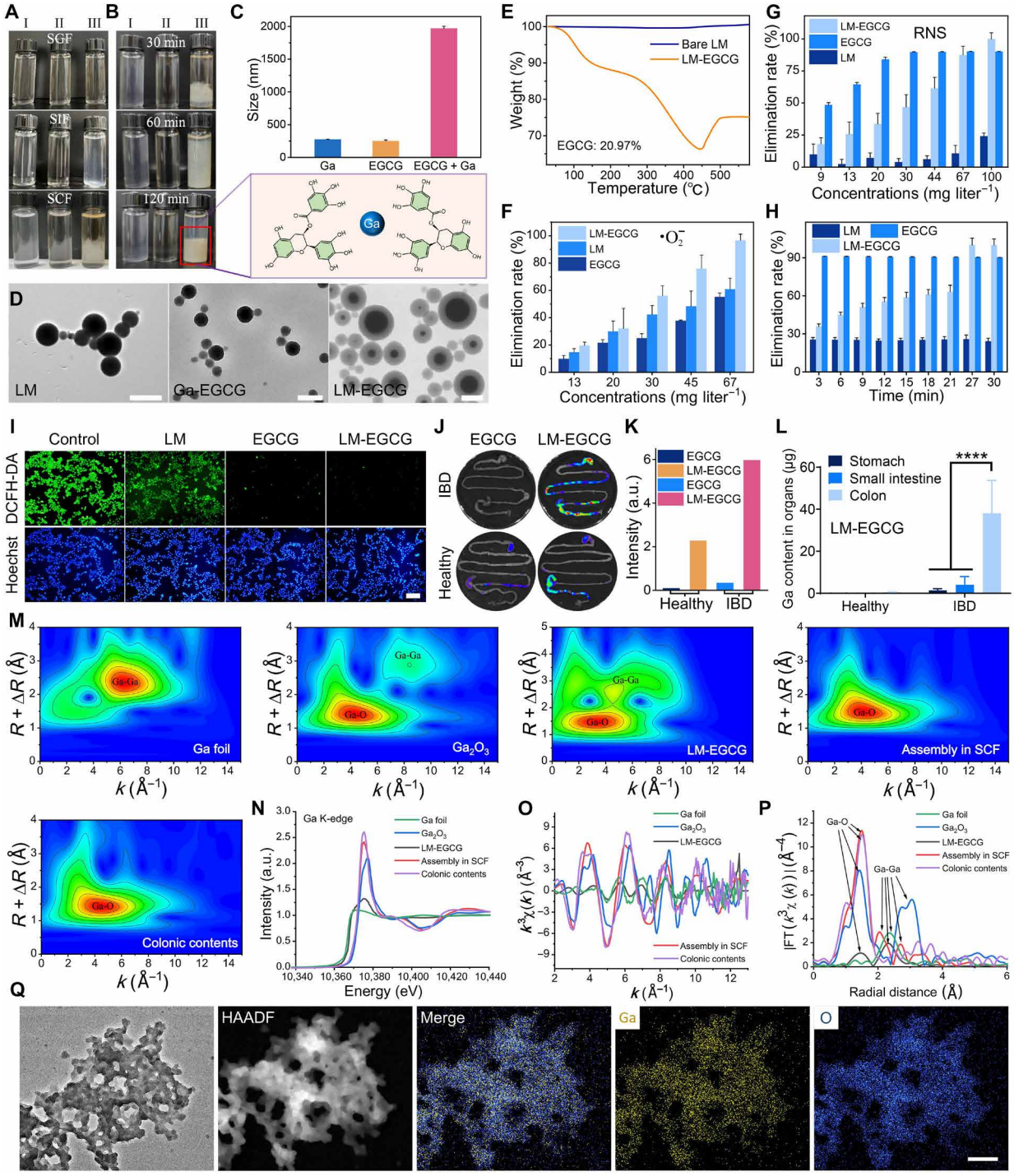

Fig. 2. LM-EGCG exerts a satisfactory RONS elimination rate and Ga^{3+} remains at the inflamed colon in DSS-treated mice. (**A** and **B**) Photographs of (A) the mixture in simulated gastric fluid (SGF), simulated intestinal fluid (SIF), and SCF and (B) the mixture in SCF at various time points. (I) Ga^{3+}, (II) EGCG, and (III) Ga^{3+} + EGCG. (**C**) Hydrodynamic size of Ga^{3+}, EGCG, and Ga^{3+} + EGCG in SCF. (**D**) Transmission electron microscopy (TEM) images of LM, Ga-EGCG, and LM-EGCG. Scale bars, 200 nm. (**E**) TG analysis of LM and LM-EGCG. (**F** and **G**) Evaluation of the (F) $\cdot O_2^-$ and (G) reactive nitrogen species (RNS) elimination rate of LM, EGCG, and LM-EGCG. (**H**) The RNS elimination capacities of LM, EGCG, and LM-EGCG at various time points. (**I**) Evaluation of the intracellular reactive oxygen species (ROS) clearance performance of LM, EGCG, and LM-EGCG. Scale bar, 100 μm. (**J** and **K**) In vivo fluorescence imaging after oral administration of Cy5.5-labeled LM-EGCG, and (K) the corresponding semiquantitative mean fluorescence intensity (MFI). (**L**) Ga content in the stomach, small intestine, and colon from healthy or DSS-treated mice after oral administration of LM-EGCG. (**M**) WT of samples Ga foil and Ga_2O_3, the mixture of EGCG and Ga in SCF, and the colonic contents from IBD mouse after oral gavage of LM-EGCG. (**N**) Ga K-edge XANES spectra of reference samples (Ga foil and Ga_2O_3), LM-EGCG, the complex collected in SCF, and the colonic contents from IBD mouse after oral gavage of LM-EGCG. (**O**) The corresponding Fourier transformation of Ga K-edge x-ray absorption fine structure (EXAFS) spectra in *k*-space. (**P**) Fourier transforms (FT) of k3-weighted Ga K-edge EXAFS spectra. (**Q**) Energy-dispersive x-ray spectroscopy element mapping images of the colonic contents from IBD mouse after oral gavage of LM-EGCG. Scale bar, 200 nm. Data are presented as means ± SD ($n = 3$). ****$P < 0.0001$, analyzed by one-way ANOVA. a.u., arbitrary units.

Elimination of RONS

The •O2$^-$-scavenging capacity of LM-EGCG was first evaluated using nitro blue tetrazolium (NBT). The absorbance of NBT solution treated with EGCG was markedly decreased with the increasing of LM-EGCG concentration (fig. S2), indicating that •O2$^-$ in NBT solutions was eliminated (Fig. 2F). As expected, the absorbance signal of LM-treated NBT solution was also decreased, indicating that LM consumes •O2$^-$ owing to its surface reducibility. Compared to EGCG or LM, more than 90% of •O2$^-$ was obliterated in LM-EGCG–treated NBT solution, suggesting the favorable antioxidative properties of LM-EGCG. Subsequently, we further investigated the reactive nitrogen species (RNS)–scavenging performance of LM-EGCG using 2,1,1-diphenyl-2-picrylhydrazyl radical (DPPH). The elimination rate of RNS was positively associated with the concentrations of LM-EGCG (Fig. 2G). Benefitting from the remarkably reduced capacity and unbound state, EGCG could efficiently eliminate RNS. Besides, because of the nanostructure of LM-EGCG, the RNS clearance efficiency of LM-EGCG was lower than dissociative EGCG at low concentrations, whereas more than 95% of RNS was effectively eliminated by LM-EGCG at the concentration of 100 μg ml^{-1}. Correspondingly, more than 90% RNS in the LM-EGCG solution was depleted after incubation for 27 min (Fig. 2H). These results demonstrate that LM-EGCG can effectively eliminate RONS.

Encouraged by the favorable RONS clearance efficiency of LM-EGCG, we further assessed its ability to scavenge intracellular RONS. Reactive oxygen species (ROS)–sensitive molecule (2′, 7′-dichlorodihydrofluorescein diacetate, DCFH-DA) probe evaluation experiments showed that compared to phosphate-buffered saline (PBS)–treated NCM460 cells, attenuated green fluorescence signals from DCFH-DA were detected in LM-treated cells, while negligible fluorescence was observed in EGCG- or LM-EGCG–treated NCM460 cells (Fig. 2I). Similarly, the RNS fluorescence probe [nitric oxide and 3-amino, 4-aminomethyl-2′, 7′-difluorescein diacetate (DAF-FM DA)] evaluation experiments confirmed that, in contrast to brilliant fluorescence in NCM460 cells treated with PBS or LM, inconspicuous green fluorescence emitted in NCM460 cells after the treatments of EGCG or LM-EGCG (fig. S3). These results indicate that EGCG or LM-EGCG could effectively clear intracellular RONS.

Accumulation of the complex at the colitis site

Before colitis treatment, the accumulation capacity of the complex of EGCG and Ga^{3+} in DSS-induced IBD mice was assessed by tracking the fluorescence from cyanine 5.5 (Cy5.5)–labeled EGCG. Compared to EGCG-treated mice (Fig. 2J), the strongest fluorescence was detected in colonic tissues in those of IBD mice after oral gavage of LM-EGCG (Fig. 2K). Besides, negligible fluorescence was observed in other organs including the heart, liver, spleen, lung, and kidney, while the strongest fluorescence was detected in colonic tissues, demonstrating an enhanced aggregation of EGCG and Ga^{3+} at inflammatory colonic tissues (fig. S4). Subsequently, we quantitatively estimated the Ga^{3+} accumulation at the colitis site by inductively coupled plasma optical emission spectrometry (ICP-OES) analysis. As assumed, plenty of Ga^{3+} was detected in the colon of the colitis mice compared to healthy mice after being orally administrated with LM-EGCG for 12 hours (Fig. 2L). Only a small amount of Ga^{3+} was detected in the stomach and small intestine of both healthy or IBD mice. Besides, negligible Ga^{3+} remained in the stomach and small intestine of IBD mice after being treated with Ga^{3+}, LM, or LM-EGCG (fig. S5A). In contrast, massive Ga^{3+} was detected in colon tissues of IBD mice after being treated with LM-EGCG, indicating that EGCG could capture Ga^{3+} to form complexes and augment the retention of Ga^{3+} at the colitis site. To verify that Ga^{3+} principally accumulated at the inflammatory tissue of the colon, the main organs (heart, liver, spleen, lung, and kidney) were collected and analyzed by ICP-OES. Except for gastrointestinal tissue, scarce Ga^{3+} was detected in the main organs through blood circulation after oral gavage of Ga^{3+}, LM, or LM-EGCG (fig. S5, B to D). These results demonstrate that EGCG could pre-target colonitis and capture Ga^{3+} to form a complex and augment the retention of Ga^{3+} at the colitis sites.

Next, to investigate the chemical state and coordination environment of the complex, we collected colonic contents from the IBD mice after oral gavage of LM-EGCG to further analyze the status of gallium by using edge-extended x-ray absorption fine structure (EXAFS), high-angle annular dark-field scanning (HAADF) TEM, and energy-dispersive x-ray spectroscopy (EDS) element mapping. According to the Fourier transformation into the *R*-space, the extended Ga K-edge EXAFS curves revealed that the main peak of the colonic contents emerged at ~1.4 Å, which was similar to Ga-O in the metal polyphenol complex in SCF rather than Ga-Ga in Ga foil or LM-EGCG (~2.5 Å) (Fig. 2M). As shown in Ga K-edge x-ray absorption near-edge structure (XANES) spectra, the absorption edge of colonic contents is nearest to the complex of EGCG and Ga in SCF, indicating that Ga species integrated with lighter atoms and positively charged with a chemical state. Consistent with the result in Ga K-edge XANES spectra, EXAFS wavelet transform (WT) analysis and Fourier transforms of *k*3-weighted Ga K-edge EXAFS spectra revealed the direct coordination of Ga-to-O atom without the formation of Ga-Ga metal–derived crystalline structures in colonic contents (Fig. 2, O and P). In addition, as the TEM and HAADF revealed, the morphology of the colonic contents was much different from LM-EGCG, and the signal of Ga element was obviously detected in the colonic contents from IBD mice after being treated with LM-EGCG by EDS element mapping (Fig. 2Q). Collectively, these results convincingly demonstrated the in situ coordination of Ga and EGCG in IBD mice after oral gavage of LM-EGCG.

Effective alleviation of DSS-induced colitis

Next, we evaluated the therapeutic efficacy of LM-EGCG against DSS-induced acute colitis (Fig. 3A). In comparison with other treatments, LM-EGCG evidently restrained the body weight loss of DSS-induced colitis mice after the secondary treatment (Fig. 3D) and reduced the hematochezia occurrence during treatment (fig. S6). In addition, the colon length of mice treated with LM-EGCG was much longer than those treated with 5-aminosalicylic acid (5-ASA), EGCG, Ga^{3+} LM, or Ga-EGCG (Fig. 3, B and C). Moreover, compared to other treatments, scarcely any red fluorescence from dihydroethidium (DHE) staining was observed in colonic tissues in IBD mice after being treated with LM-EGCG (fig. S7A). As shown in the results of terminal deoxynucleotidyl transferase–mediated deoxyuridine triphosphate nick end labeling (TUNEL), consistent with mice in the healthy group, ignorable green fluorescence was detected in LM-EGCG–treated mice (fig. S7B), confirming that LM-EGCG could protect the intestinal villus from further injury. Furthermore, LM-EGCG treatment furthest augmented the

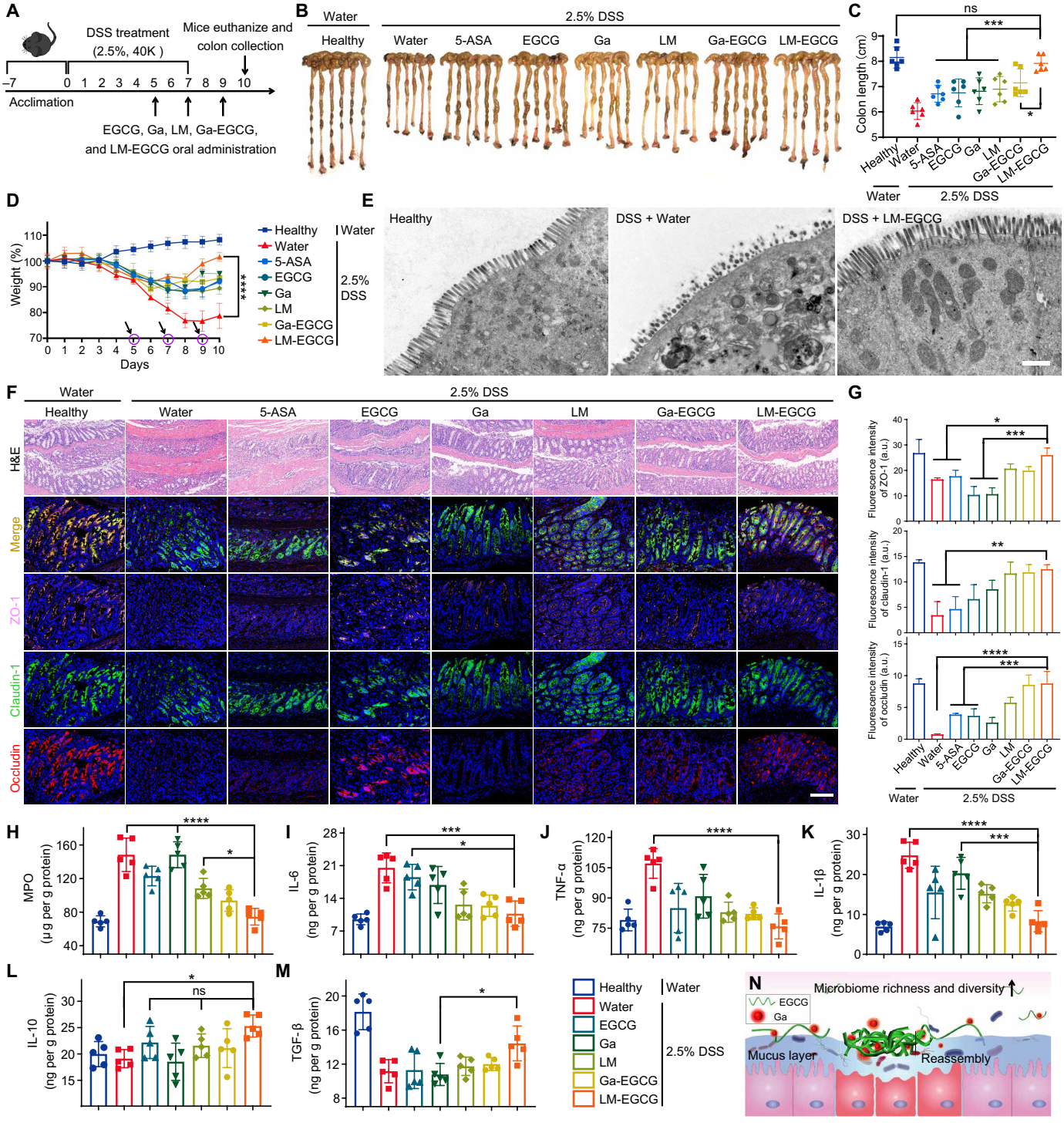

Fig. 3. LM-EGCG efficiently mitigates DSS-induced colitis in a murine model. (**A**) The C57BL/6 mice were orally administered with water, 5-ASA, EGCG, Ga^{3+}, LM, Ga-EGCG, or LM-EGCG on days 5, 7, and 9 after being treated with water or 2.5% DSS-containing water for 7 days. (**B** and **C**) Photographs of colon tissues obtained after various treatments on day 10 and (C) the corresponding colon length ($n = 6$). (**D**) Daily body weight changes in each group for 10 days. (**E**) Bio-TEM images of colon tissues obtained from healthy, DSS-treated, or DSS + LM-EGCG–treated mice. Scale bar, 1 μm. (**F** and **G**) The colon tissues were collected for immunofluorescence staining of ZO-1 (pink), claudin-1 (green), and occludin (red) at the end of treatment and (G) the corresponding semiquantitative MFI analysis. Scale bar, 100 μm. (**H** to **M**) Relative (H) myeloperoxidase (MPO), (I) interleukin-6 (IL-6), (J) tumor necrosis factor–α (TNF-α), (K) IL-1β, (L) IL-10, and (M) transforming growth factor–β (TGF-β) levels in the collected colon tissues by enzyme-linked immunosorbent assay (ELISA) analysis ($n = 5$). (**N**) Schematic diagram of the mechanism of LM-EGCG for colitis remission. Data are presented as means ± SD. *$P < 0.05$, **$P < 0.01$, ***$P < 0.001$, and ****$P < 0.0001$, analyzed by [(C), (G), and (H) to (M)] one-way or (D) two-way ANOVA. ns, not significant.

expression level of proliferating cell nuclear antigen in DSS-induced colitis mice (fig. S7C), suggesting that the impaired colonic tissues were renovated after oral gavage of LM-EGCG.

Furthermore, the colon tissues were analyzed by Bio-TEM after treatment to assess intestinal villus recovery of DSS-induced colitis mice (Fig. 3E). Compared to healthy mice that fed with water, extensive damage to intestinal villi was revealed in the mice fed with 2.5% DSS in drinking water, indicating apparent damages to the intestinal tissue of DSS-induced colitis mice. Notably, the length or morphology of damaged intestinal villi in DSS-induced colitis mice was restored after being treated with LM-EGCG, revealing LM-EGCG's therapeutic effects against DSS-induced colitis. Meanwhile, immunofluorescent staining analysis on expression of tight junction-correlative proteins, including zonula occludens-1 (ZO-1) (pink; fig. S8), claudin-1 (green; fig. S9), and occludin (ted; fig. S10), was used to assess the repair effects of various treatments on DSS-inflamed colonic epithelium (Fig. 3F). Notably, brightest pink, green, and red fluorescence were concurrently observed on the healthy mice and DSS-induced colitis mice that orally administered with LM-EGCG, while relatively feeble fluorescence was detected in other control groups, including 5-ASA, EGCG, LM, and Ga-EGCG treatment (Fig. 3G), indicating that LM-EGCG could normalize the expression of the tight junction-associated proteins and efficiently repair the DSS-inflamed intestinal epithelial barrier in DSS-induced colitis mice.

Remission of colonic inflammation

The overexpression of pro-inflammatory cytokines, such as interleukin-6 (IL-6), IL-1β, and tumor necrosis factor–α (TNF-α), could activate an inflammatory cascade response in IBD. We thus analyzed the trends of pro-inflammatory or anti-inflammatory cytokines expression levels in colonic tissues after various treatments using enzyme-linked immunosorbent assay (ELISA). As expected, compared to other control groups, DSS-induced colitis mice orally administered with LM-EGCG not only furthest decreased the local level of IBD-associated myeloperoxidase (MPO) in the colon (Fig. 3H) but also reduced the expression of pro-inflammatory cytokines, including IL-6, TNF-α, and IL-1β, while increasing the expression of anti-inflammatory cytokines IL-10 and transforming growth factor–β (TGF-β) (Fig. 3, I to M). To further evaluate the effect of LM-EGCG on inflammatory regulation in DSS-induced colitis mice, we detected the local levels of a pro-inflammatory M1 macrophages' marker, inducible nitric oxide synthase (iNOS; red), and an M2 macrophages' marker, arginase-1 (Arg-1; green), in colon tissue by immunofluorescence analysis (fig. S11). Consistent with the result of ELISA, low levels of Arg-1 and iNOS were detected in DSS-induced colitis mice with oral administration of LM-EGCG compared to other control groups. Besides, according to the results in immunohistochemistry analysis, LM-EGCG evidently reduced the CD86 level, which was similar to those of colonic tissues in healthy mice (fig. S12), suggesting that LM-EGCG could evidently extinguish the hyperactive inflammatory response in DSS-induced colitis mice. These results strongly indicate that LM-EGCG could efficiently lower the pro-inflammatory cytokines and inactivate inflammatory responses, thereby relieving DSS-induced IBDs.

Therapeutic mechanisms of LM-EGCG on IBD

To further illustrate the therapeutic mechanism of the LM-EGCG to DSS-induced colitis, transcriptome analysis of colonic tissues was conducted at the end of treatment. As shown in Fig. 4 (A and B), compared to the healthy mice, 966 up-regulated genes and 1138 down-regulated genes in DSS-induced colitis mice were detected. Meanwhile, 744 genes were up-regulated, and 960 genes were down-regulated after the regulation of LM-EGCG. The results in the Kyoto Encyclopedia of Genes and Genomes (KEGG) pathway enrichment analysis showed that the IL-17, inflammatory response, and TNF signaling pathways are overexpressed in DSS-induced colitis mice compared to healthy mice or LM-EGCG–treated IBD mice (Fig. 4, D and E), suggesting that those of signaling pathways are highly associated with the therapeutic mechanisms of LM-EGCG. Furthermore, compared to healthy mice, the normalized heatmap revealed that the genes related to inflammatory response were highly expressed in DSS-induced colitis, which was evidently decreased after LM-EGCG treatment (Fig. 4C). Similarly, LM-EGCG treatment decreased the expression level of the genes related to ROS in DSS-induced colitis mice (Fig. 4F). Besides, according to KEGG pathway function enrichment, the LM-EGCG treatment increased the expression level in Wnt signaling pathway, which was beneficial to repair of intestinal epithelial damage (*46*), in comparison with DSS-induced colitis mice (Fig. 4G). Synchronously, the tight junction-associated genes were markedly up-regulated in DSS-induced mice under LM-EGCG treatment (Fig. 4H). Consistently, the above evidence convincingly indicated that LM-EGCG could effectively eliminate oxidative stress, relieve inflammation, and recover the intestinal barrier.

Modulation of LM-EGCG on gut microbiome

Reinstating disordered gut microbiota via imposing restrictions on the abnormal expansion of cantankerous microbes is beneficial to relieving IBD. Encouraged by the favorable alleviation of colonic inflammation, we investigated the gut microbiome variation by 16*S* ribosomal RNA (rRNA) gene sequencing in the V4 region of fecal samples from the experimental mice after various treatments on day 10. Compared to DSS-induced colitis mice treated with EGCG or 5-ASA, bacterial richness (observed operational taxonomic unit richness) and diversity (Shannon and Simpson) in DSS-induced colitis mice treated with Ga-based nano-agents were notably increased and similar to healthy mice (Fig. 5, A to D). The principal coordinates analysis revealed that the composition of gut microbiota in DSS-induced colitis mice treated with LM-EGCG was closest to the healthy mice (Fig. 5F). Furthermore, the analysis of microbiota composition revealed that LM-EGCG treatment decreased the relative abundance of *Enterobacteriaceae* and *Bacteroidaceae* but increased the proportion of *Lactobacillaceae* and *Verrucomicrobiaceae* (Fig. 5E).

Unexpectedly, among the variation of microbiota composition, the overexpansion of *Escherichia_Shigella* (known to induce diarrhea and IBDs) and *Bacteroides* (known to be associated with the progression of DSS-induced IBDs) was terminated in DSS-induced colitis mice with oral administration of LM-EGCG (Fig. 5, G and H), while the populations of *Akkermansia muciniphila* (*AKK*; known to protect intestinal barrier functions) and *Bifidobacterium* (known for increasing expression levels of junction proteins) were increased (Fig. 5, I and J). Moreover, for further investigation of the impact of Ga^{3+} on gut microbiota, we counted the colony-forming units (CFUs) of *Escherichia coli* after Ga^{3+} treatment (Fig. 5K). Approximately 60% of *E. coli* was inhibited as the concentration of Ga^{3+} reached 64 mg $liter^{-1}$ (Fig. 5L and fig. S13). On the contrary, compared with the aseptic culture medium containing

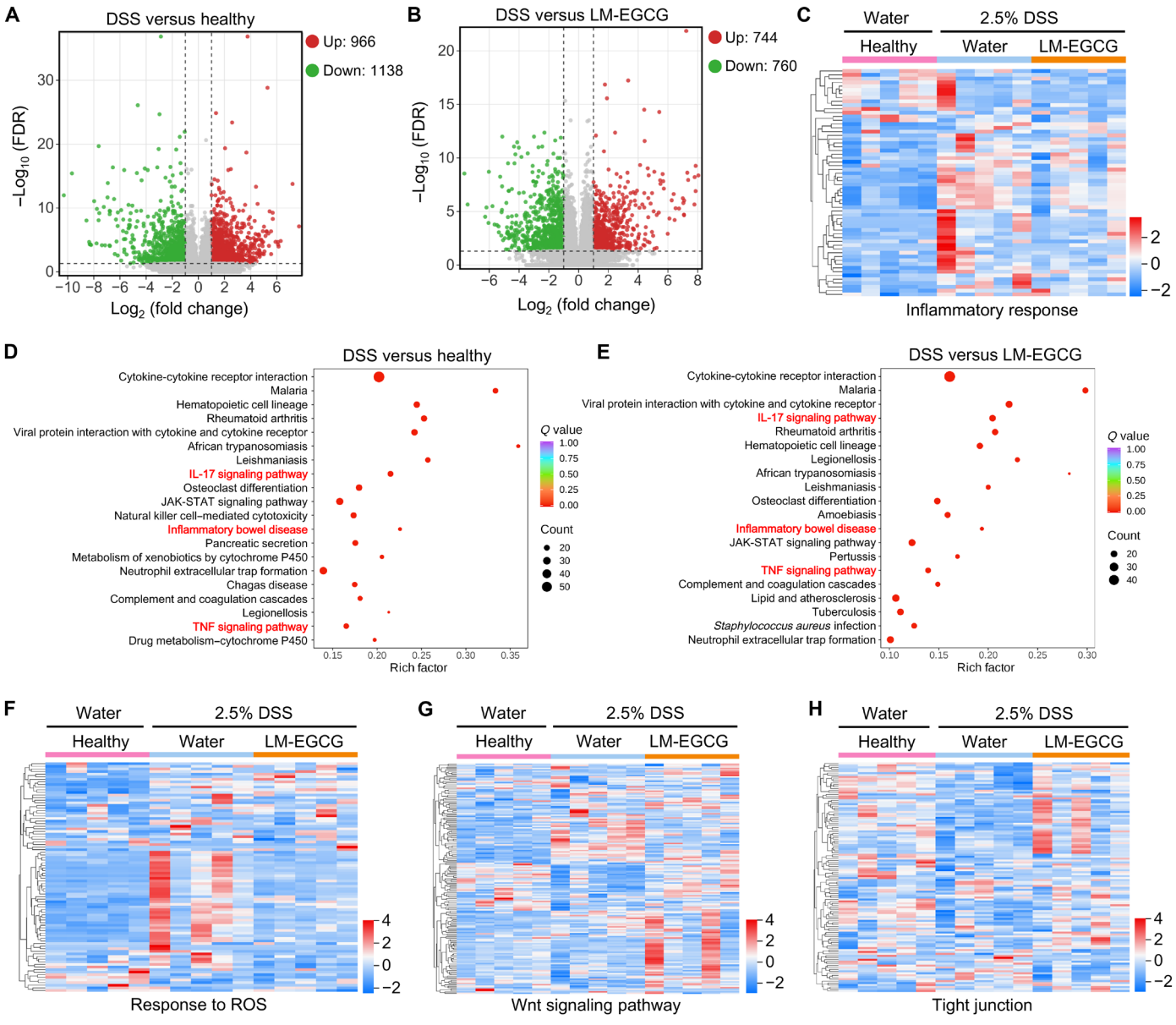

Fig. 4. Transcriptomic analysis of DSS-induced colitis in mice after the regulation of LM-EGCG. (**A** and **B**) Volcano plot exhibiting the differentially expressed genes in (A) the comparison of DSS with the healthy group and (B) the DSS versus the LM-EGCG–treated group from RNA sequencing data (red: up-regulated genes; green: down-regulated genes). (**C**) Heatmap analysis of the expression of the inflammatory response genes in mice after being treated with LM-EGCG. (**D** and **E**) Kyoto Encyclopedia of Genes and Genomes pathway enrichment analysis of the up-regulated genes in (D) the comparison of DSS with the healthy group and (E) in the DSS versus the LM-EGCG–treated mice. The 20 most significantly enriched pathways were shown. (**F** to **H**) Heatmap analysis of the expression of the (F) response to ROS, (G) Wnt signaling pathways, and (H) cell tight junction signaling pathways in the healthy, IBD, LM-EGCG–treated mice. Data represent at least five independent replicates.

Ga^{3+} (fig. S14A), the *AKK*-inoculated culture medium was evidently turbid (fig. S14B). Meanwhile, the corresponding OD_{600} (optical density at 600 nm) of *AKK* was almost unchanged with the increase of Ga^{3+} concentration, indicating that Ga^{3+} showed an insignificant impact on the growth and proliferation of *AKK* (fig. S14C). Collectively, these results indicate that LM-EGCG is capable of ameliorating disordered gut microbiota, and is beneficial for improving colitis.

Short-chain fatty acids (SCFAs), produced by probiotic gut microbiota, have commendable anti-inflammatory capacities and can enhance the function of the regulatory T cell to prevent an excessive immune response for effective amelioration of colitis (*47*, *48*). Encouraged by the gut microbiome modulation, the feces SCFA levels in experimental mice were investigated after the secondary gavage of LM-EGCG. As shown in Fig. 5M, LM-EGCG treatment significantly increased the total SCFA levels in comparison with water-treated IBD mice. Particularly, LM-EGCG treatment markedly improved the abundance of acetic, *n*-butyric, and propionic acid, which approached those of mice in the healthy group (Fig. 5M and fig. S15). Moreover, the production of branched SCFAs, including

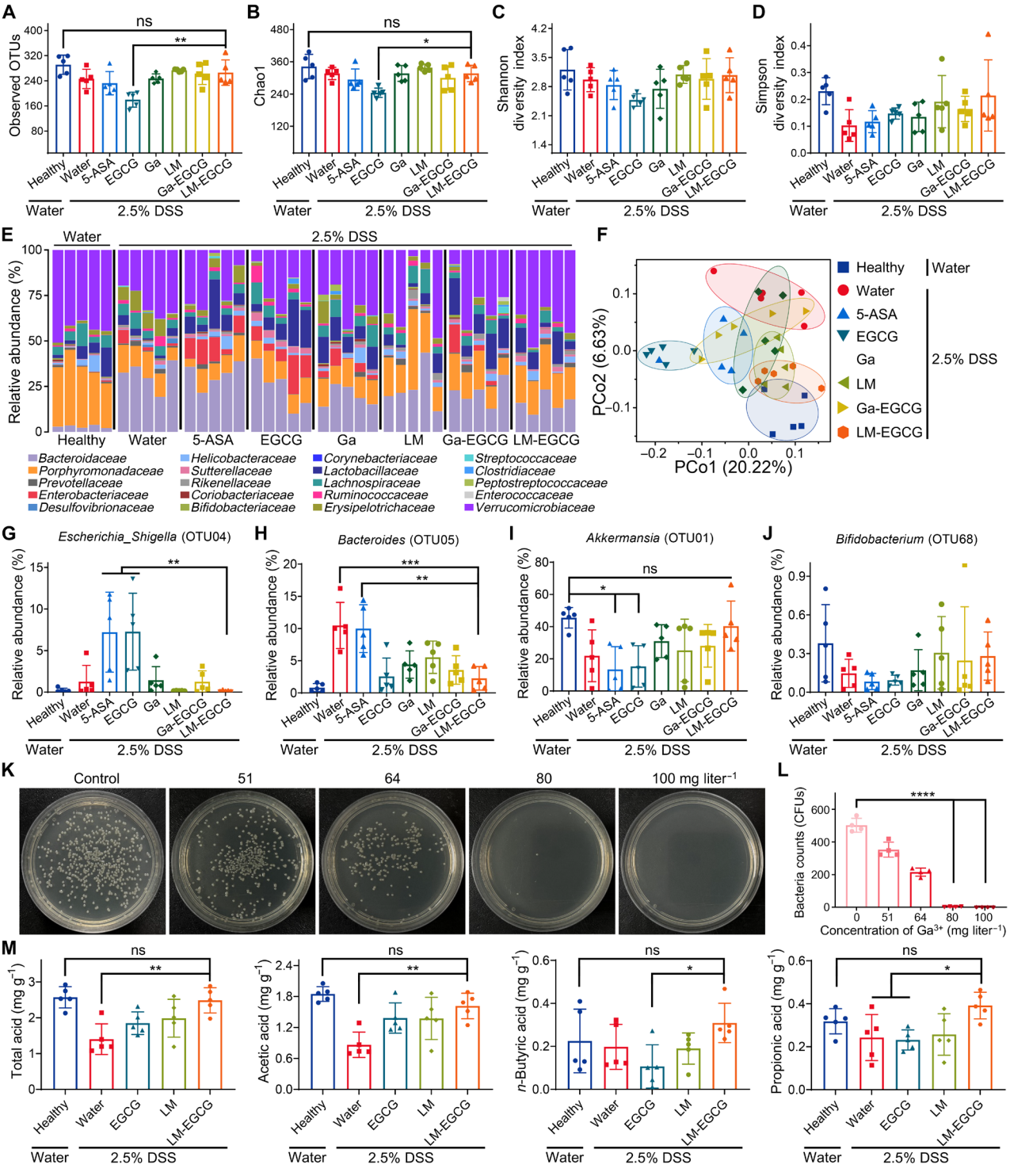

Fig. 5. LM-EGCG regulates the gut microbiome dysbiosis and improves the intestinal microenvironment. Feces from the treated mice were collected for gut microbiome analysis by 16*S* rRNA sequencing. (**A**) Estimation of microbial community observed operational taxonomic unit (OTU) richness. (**B** to **D**) Alpha-diversity was displayed by (B) chao1, (C) Shannon, and (D) Simpson. (**E**) Relative abundance of the gut microbiome is presented at family-level taxonomy. (**F**) Principal coordinates analysis (PCoA) illustrating the β-diversity of the gut microbiome. Each point represents each mouse. (**G** to **J**) Relative abundance of selected taxa (G) *Escherichia_Shigella*, (H) *Bacteroides*, (I) *Akkermansia*, and (J) *Bifidobacterium*. (**K** and **L**) Photographs of bacterial colonies of *E. coli* after being treated with different concentrations of Ga^{3+}, and (L) the corresponding colony count. (**M**) Short-chain fatty acid levels in feces from experimental mice after various treatments by using gas chromatography–mass spectrometry. Data are presented as means ± SD ($n = 5$). **P* < 0.05, ***P* < 0.01, ****P* < 0.001, and *****P* < 0.0001, analyzed by one-way ANOVA.

isobutyric, isovaleric, and 2-methylbutyric acid, were also elevated after LM-EGCG treatment (fig. S15). In short, LM-EGCG treatment ameliorated the gut microbiota to promote the generation of SCFA levels, which could contribute to the amelioration of colitis in mice.

Amelioration of colitis after antibiotic pretreatment

Then, we assessed the efficacy of LM-EGCG against colitis in mice after pretreatment with a cocktail of antibiotics. The mice were orally administered with a cocktail of antibiotics for 5 days to disrupt gut commensal microbes before being fed with DSS (Fig. 6A). Although LM-EGCG could suspend the further shortening of colon length, the colon was still significantly shorter than the colon of healthy mice (Fig. 6, B and C). LM-EGCG treatment increased the expression of tight junction-associated proteins (Fig. 6, D and E), including ZO-1 (pink; fig. S16), claudin-1 (green; fig. S17), and occludin (red; fig. S18), and restored the damaged intestinal villi

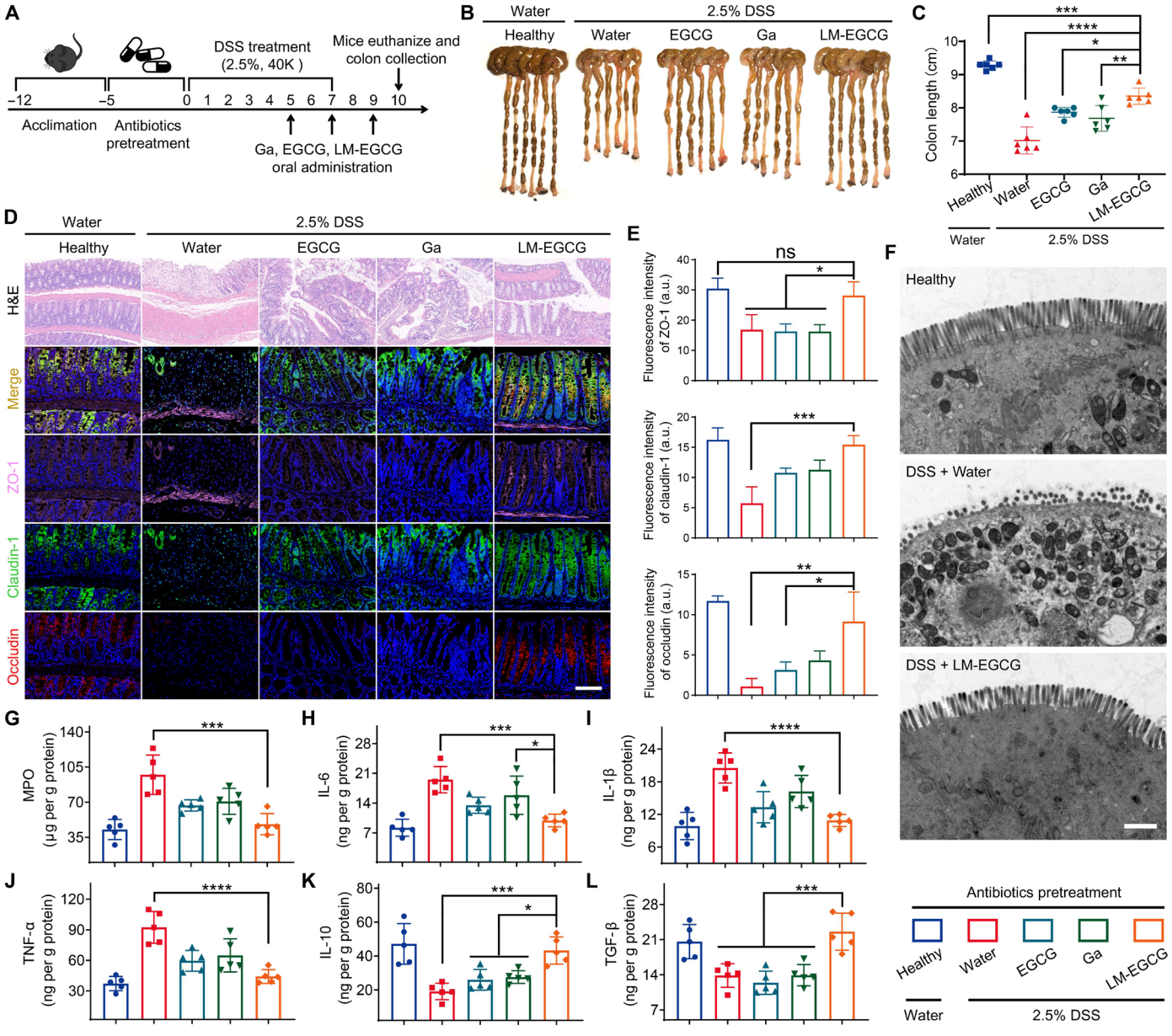

Fig. 6. LM-EGCG mitigates colitis in a murine model that was pretreated with a cocktail of antibiotics. (**A**) C57BL/6 mice were pretreated with a cocktail of antibiotics for 5 days and then orally administered with water or EGCG, Ga^{3+}, or LM-EGCG on days 5, 7, and 9 after being treated with water or 2.5% DSS-containing water for 7 days. (**B** and **C**) Photographs of colon tissues obtained after various treatments on day 10 and (C) the corresponding colon length ($n = 6$). (**D** and **E**) The colon tissues were collected for immunofluorescence staining (D) of ZO-1 (pink), claudin-1 (green), and occludin (red) at the end of treatment, and (E) the corresponding semiquantitative MFI analysis. Scale bar, 100 μm. (**F**) Bio-TEM images of colon tissues obtained from healthy, DSS-treated, or DSS + LM-EGCG–treated mice. Scale bar, 1 μm. (**G** to **L**) Relative (G) MPO, (H) IL-6, (I) IL-1β, (J) TNF-α, (K) IL-10, and (L) TGF-β levels in the collected colon tissues by ELISA analysis ($n = 5$). Data are presented as means ± SD. *$P < 0.05$, **$P < 0.01$, ***$P < 0.001$, and ****$P < 0.0001$, analyzed by one-way ANOVA.

(Fig. 6F). Compared to control groups, DSS-induced colitis mice treated with LM-EGCG not only furthest decreased the local level of IBD-associated MPO in the colon (Fig. 6G) but also reduced the expression of pro-inflammatory cytokines, including IL-6, TNF-α, and IL-1β, while increasing the expression of anti-inflammatory cytokines IL-10 and TGF-β (Fig. 6, H to L). Furthermore, LM-EGCG treatment markedly weakened the fluorescence from the pro-inflammatory M1 macrophage marker, iNOS (red), and the M2 macrophage marker, Arg-1 (green), in comparison with other control groups (fig. S19). Together, LM-EGCG treatment could weaken the inflammatory response and restore the intestinal barrier in DSS-induced colitis mice, whereas the efficacy of LM-EGCG against DSS-induced colitis was discounted without the assistance of modulated gut microbiome (*4*, *49*).

Amelioration of severe colitis with delayed treatment

Encouraged by the excellent gut microbiota regulation and colitis amelioration capacity of LM-EGCG, we further investigated LM-EGCG against the severe colitis induced by DSS. Before LM-EGCG treatment, the mice were fed with 2.5% DSS containing water for 10 days (Fig. 7A). At the end of DSS feeding, various agents were orally administrated on days 10, 12, and 14. LM-EGCG treatment halted the sharp downward tendency of body weight of colitis mice, which then restored to the beginning of the DSS feeding (fig. S20). Understandably, LM-EGCG not only renovated the impaired colon tissues (Fig. 7B), which approached the healthy mice (Fig. 7C), but also commendably increased the expression of the tight junction-associated proteins (Fig. 7, D and E), including ZO-1 (pink; fig. S21), claudin-1 (green; fig. S22), and occludin (red; fig. S23). Furthermore, compared to control groups, DSS-induced colitis mice treated with LM-EGCG not only recovered the damaged intestinal villi (Fig. 7F) but also maximally decreased the local level of IBD-associated MPO in the colon (Fig. 7G) and reduced the expression of pro-inflammatory cytokines, including IL-6, TNF-α, and IL-1β. Simultaneously, the expression of anti-inflammatory cytokines IL-10 and TGF-β was increased (Fig. 7, H to L). Similarly, LM-EGCG treatment sharply weakened the fluorescence from the pro-inflammatory M1 macrophage marker, iNOS (red), and the M2 macrophage marker, Arg-1 (green), in comparison with other control groups (fig. S24). Satisfactorily, LM-EGCG treatment could weaken the inflammatory response and restore the intestinal barrier in DSS-induced colitis mice, thus relieving DSS-induced IBD.

Biocompatibility of LM-EGCG

First, the cell viability after incubation with various agents was investigated. Markedly, more than 80% of NCM460 cells were alive when the concentration of Ga^{3+} reached 400 μg ml^{-1} (Fig. 8A). Correspondingly, almost all NCM460 cells were alive after being treated with 100 μg ml^{-1} EGCG (the loading rate of EGCG from LM-EGCG was about 20%) (Fig. 8B). As expected, Ga-EGCG or LM-EGCG exhibited no impact on the growth and proliferation of NCM460 cells (Fig. 8C). Consistent with the results detected by cytotoxicity assay, massive green fluorescence was observed from living cells while scarcely any of red fluorescence was detected in those of NCM460 cells even the concentration of LM-EGCG reached up to 800 μg ml^{-1} (Fig. 8E and fig. S25), convincingly demonstrated that Ga^{3+} or LM-EGCG was nontoxic. In addition, compared with the control group, no apparent hemolysis was observed in those blood samples incubated with EGCG, Ga^{3+}, Ga-EGCG, or LM-EGCG, respectively, even though the concentration of the agents arrived at 400 μg ml^{-1} (Fig. 8F and fig. S26).

Thereafter, in consideration of the favorable degradation property in the acid environment of LM (*50*), we detected the Ga content in blood, urine, and excretion from normal mice after being orally treated with LM-EGCG. Apparently, insignificant Ga^{3+} was detected in blood and urine from DSS-induced colitis mice after oral gavage of LM-EGCG (fig. S27). The majority of Ga^{3+} in LM or LM-EGCG was excreted via excrement in healthy mice after oral gavage of the above agents for 24 hours (Fig. 8D). Moreover, after the delayed treatment, the hematoxylin and eosin (H&E) staining analysis of major organs (heart, liver, spleen, lung, and kidney) revealed that no pathological abnormalities in the organs were detected, suggesting that LM-EGCG had no obvious tissular toxicity on those of experimental mice during the treatment (fig. S28). Furthermore, the liver and kidney functions were applied to further assess the biosafety of LM-EGCG by detecting the crucial detection indicators containing creatinine (Crea), blood urea (Urea), glucose (GLU), alanine aminotransferase (ALT), total protein (TP), alkaline phosphatase (ALP), albumin (ALB), and total bilirubin (TBIL) (*51*). As important biomarkers of kidney function, Crea, Urea, and GLU were rectified to normal range after the remission of enteritis in comparison with other control groups (Fig. 8, G to I). Similarly, the important markers of liver function including ALT, TP, ALP, ALB, and TBIL in LM-EGCG–treated mice were much closer to the healthy mice, demonstrating that LM-EGCG had no visible hepatic toxicity in mice (Fig. 8, J to N). Collectively, these results confirmed that the constructed LM-EGCG had negligible side effects and good biocompatibility for biomedical applications.

DISCUSSION

IBDs, including ulcerative colitis and Crohn's disease, are chronic inflammatory diseases of the gastrointestinal tract, which will markedly lower the quality of life of patients and have been an emerging challenge for public health worldwide (*52*, *53*). The overproduced ROS and overexpansion of profitless bacteria are typical pathological features of colitis (*54*). The hyperactive ROS not only provokes the inflammatory cells to produce a great deal of ROS during the progress of colitis to hurt the intestinal epithelial cells but also restrains the colonization of beneficial bacteria at the inflammatory site (*55*). The abnormal expansion of harmful bacteria, such as *E. coli*, will occupy the ecological niches to prevent the colonization of beneficial bacteria and the reprogramming of the microbiome during inflammation, thereby impeding the recovery of the colitis microenvironment (*56*, *57*). In our work, the reductive EGCG, a polyphenol in green tea (*42*), was applied to eliminate the overproduced ROS. Meanwhile, Ga-based LM was used as an antibiotic-free intestinal flora regulator to modulate the dysregulated microbiome for effective remission of DSS-induced colitis. Our results indicate that the strategy of working along both lines to eliminate the overproduced ROS and simultaneously modulate intestinal flora could efficiently ameliorate the colitis microenvironment.

Targeting drug delivery in response to the pathological microenvironment provides opportunities for diminishing the off-target systemic side effects and improving the therapeutic effect of IBD treatments. The inflamed colon is characterized by the imbalance of the gut microbiome, hyperactive immune responses, elevated levels of ROS, and enrichment of positively charged proteins

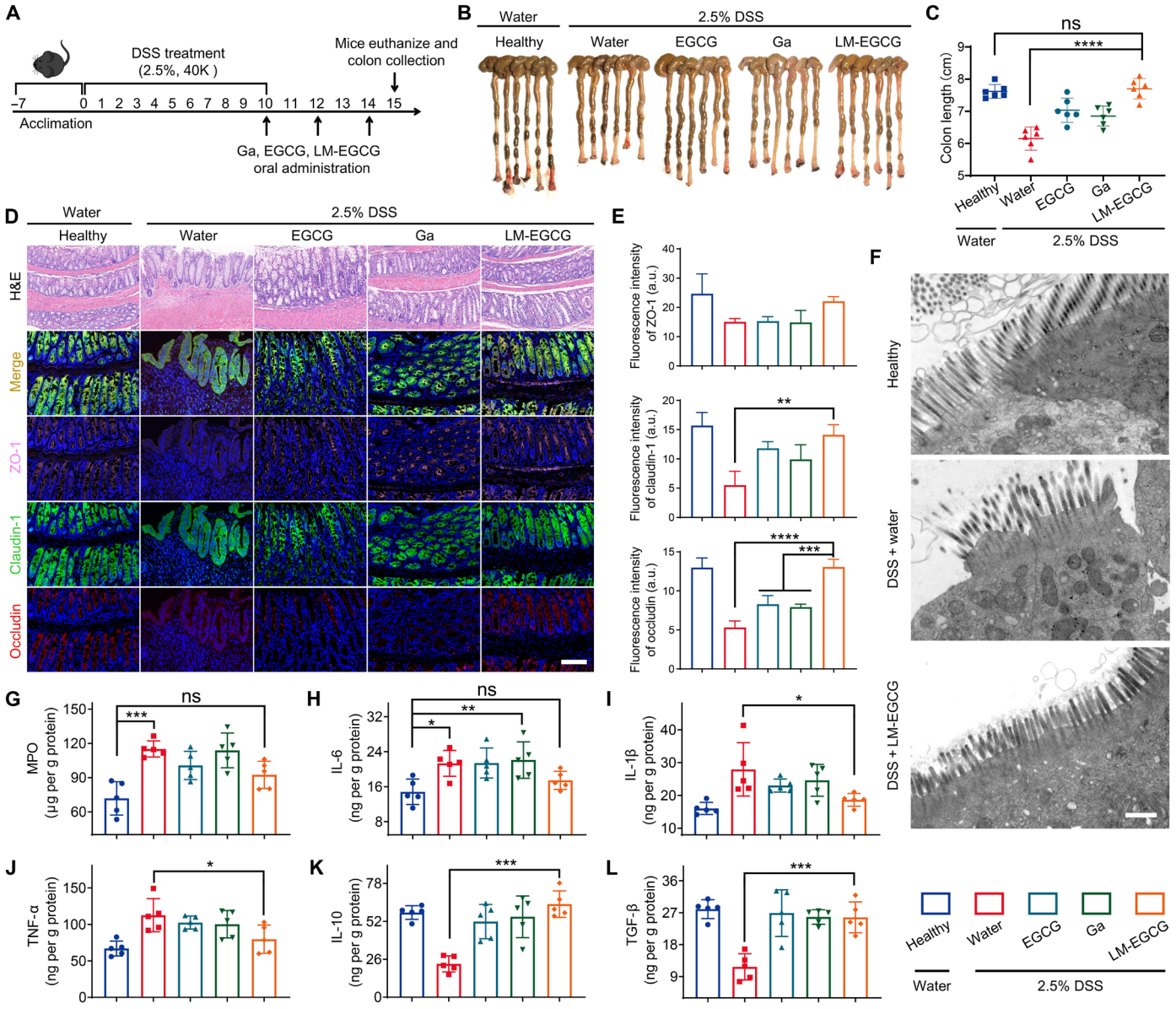

Fig. 7. LM-EGCG exerts satisfactory therapeutic efficacy in a murine model of DSS-induced colitis with a delayed therapeutic setting. (**A**) C57BL/6 mice were orally administered with water or EGCG, Ga^{3+}, or LM-EGCG on days 10, 12, and 14 after being treated with water or 2.5% DSS-containing water for 10 days. (**B** and **C**) Photographs of colon tissues obtained after various treatments on day 10 and (C) the corresponding colon length ($n = 6$). (**D** and **E**) The colon tissues were collected for immunofluorescence staining of ZO-1 (pink), occludin-1 (green), and occludin (red) at the end of treatment and (E) the corresponding semiquantitative MFI analysis. Scale bar, 100 μm. (**F**) Bio-TEM images of colon tissues obtained from healthy, DSS-treated, or DSS + LM-EGCG–treated mice. Scale bar, 1 μm. (**G** to **L**) Relative (G) MPO, (H) IL-6, (I) IL-1β, (J) TNF-α, (K) IL-10, and (L) TGF-β levels in the collected colon tissues by ELISA analysis ($n = 5$). Data are presented as means ± SD. *$P < 0.05$, **$P < 0.01$, ***$P < 0.001$, and ****$P < 0.0001$, analyzed by one-way ANOVA.

(*58*, *59*). Exploiting ROS-induced targeting retention of therapeutic agents at inflammatory sites is an optional approach to meet the medical need of improving drug bioavailability (*60*, *61*). Green tea polyphenol (EGCG) has a polyhydroxy structure that can adhere to the innate amine, thiol, carboxyl groups, and electropositive biomolecule making EGCG a potential therapeutic drug for gastrointestinal disease (*43*–*45*). In addition to the adhesion behavior, the EGCG would be polymerized during the process of scavenging ROS. In this study, we used EGCG as a pre-targeting module to accumulate at the inflammation site for scavenging the overproduced ROS and synchronously capture the metal ions (Ga) to form metal-phenolic complexes in situ at the colonic microenvironment. The result revealed that the detained metal-phenolic complexes elevated the gathering of EGCG and Ga at the colitic area to balance the oxidative stress and protect the damaged intestinal barrier from graver injury.

Gut microbiota dysbiosis is closely related to the progress of colitis, and increasing evidence has denoted that regulating the gut

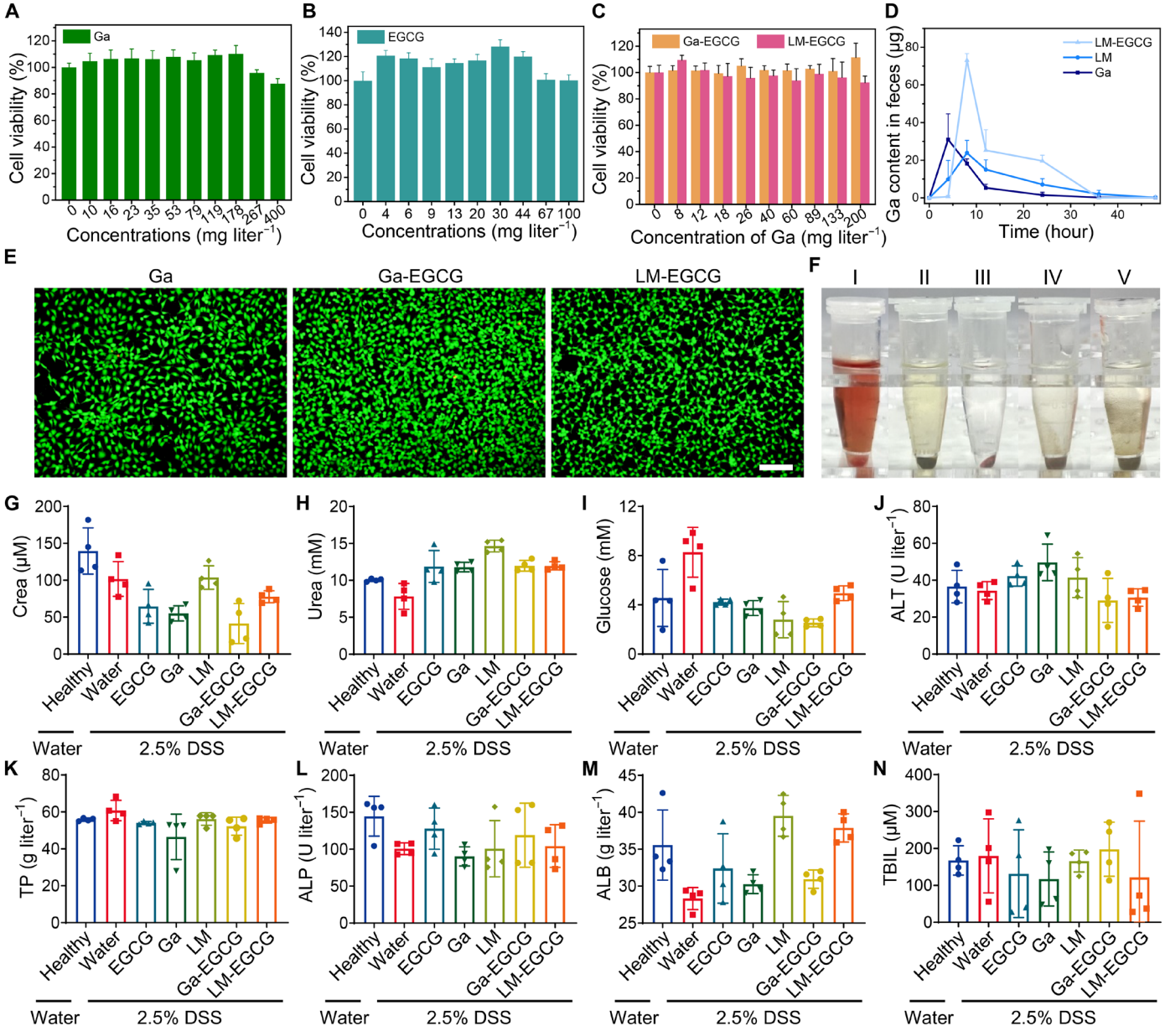

Fig. 8. LM-EGCG shows favorable biosecurity. (**A** to **C**) In vitro cell viabilities of NCM460 cells (normal colonic epithelial cells) after incubation with different concentrations of (A) Ga^{3+}, (B) EGCG, and (C) Ga-EGCG or LM-EGCG for 24 hours. (**D**) Ga content in feces after oral administration of Ga^{3+}, LM, or LM-EGCG. (**E**) Fluorescence images of Ga^{3+}, Ga-EGCG, or LM-EGCG–treated NCM460 cells stained with calcein AM (green fluorescence, living cells) and PI (red fluorescence, dead cells). Scale bar, 100 μm. (**F**) Photographs of the microcentrifuge tubes containing blood samples with various treatments. (I) H_2O, (II) EGCG, (III) Ga^{3+}, (IV) Ga-EGCG, and (V) LM-EGCG. (**G** to **I**) Renal function was evaluated by monitoring the (G) creatinine (Crea), (H) blood urea (Urea), and (I) glucose levels in the blood after various treatments. (**J** to **N**) Liver function was evaluated by monitoring the important markers of (J) alanine aminotransferase (ALT), (K) total protein (TP), (L) alkaline phosphatase (ALP), (M) albumin (ALB), and (M) total bilirubin (TBIL) levels in the blood after various treatments.

microbiota is highly beneficial to the alleviation of IBDs (*62*, *63*). The inconducive microbes became dominant bacteria and the population of beneficial bacteria decreased during the occurrence of colitis (*64*, *65*). Toward the goal of frenzied expansion, the pathogenic bacteria require a lot of nutriment to meet their high level of metabolism. As an indispensable nutrient for bacterial survival, proliferation, and bacterial infection, iron is involved in many vital metabolic processes, including energy generation and DNA synthesis (*66*). The biological systems of bacteria are unable to distinguish gallium from iron ions and will specifically take in gallium through iron ion uptake pathways, making gallium a potential "tool" for bacterial regulation. We used Ga-based LM, which could be degraded in an acidic environment and released Ga^{3+}, to modulate the gut microbiome for the alleviation of colitis. Our results showed that, with the assistance of gut microbiome modulation, the designed LM nano-agents could efficiently relieve DSS-induced colitis.

In summary, in consideration of the poor targeting accumulation capacity of conventional drugs that are difficult to concurrently modulate the dysregulated microbiome and simultaneously obliterate overproduced RONS in IBDs, we propose an amplifying targeting strategy to enhance the accumulation of therapeutic agents at the colitis site for IBDs remission. First, we validated the treatment efficacy of LM-EGCG against colitis in the process of forming enteritis. Then, to examine the contribution of intestinal flora to colitis, we examined the efficacy of LM-EGCG against colitis in mice after pretreatment with a cocktail of antibiotics. After that, the efficacy of LM-EGCG in delayed therapy was assessed on mice after being fed with 2.5% DSS containing water for 10 days. The consequences of toxicological evaluation demonstrate that LM-EGCG had negligible side effects on the experimental mice, indicating that LM is a promising candidate for a broad variety of biomedical applications including IBD alleviation. However, the lack of large animal models in the evaluation of therapeutic efficacy is one limitation of the current study due to the limitations of the mouse model in elucidating complex human pathology. We will further investigate the therapeutic efficacy of an LM-based system against colitis in large animals. In addition, in-depth studies of the molecular mechanisms in gut microbiome modulation in situ and systematic biocompatibility evaluation are necessary before the further application of LM-based nano-agents.

MATERIALS AND METHODS

Reagents

Gallium-indium eutectic (99.99% LM) was purchased from Alfa Esha (China) Chemical Co., LTD. Methoxy poly(ethylene glycol) thiol (mPEG-SH; $M_w = 5$ kDa) was purchased from Shanghai Ponsure Biotech, Inc. EGCG, 5-ASA, 1, DPPH, NBT, and 3-(4,5-dimeth ylthiazol-2-yl)-2,5-diphenyl-2H-tetrazolium bromide (MTT) were purchased from Aladdin Biochemical Technology Co., Ltd. (Shanghai, China). DSS salt colitis grade (36,000 to 50,000 Da) was purchased from MP Biomedicals (Santa Ana, CA, USA). Dulbecco's modified Eagle's medium (DMEM) and fetal bovine serum (FBS) were purchased from Gibco Laboratories (Grand Island, NY, USA). DCFH-DA, DAF-FM DA, calcein-AM (acetoxymethyl), bicinchoninic acid (BCA) kit, and propidium iodide (PI) were purchased from Beyotime Biotech Inc. (Shanghai, China). Radio immunoprecipitation assay (RIPA) was purchased from Wuhan Boerfu Biotechnology Co., Ltd. (Hubei, China). ELISA kits were purchased from 4A Biotech Co., Ltd. (Jiangsu, China). Metronidazole, vancomycin, neomycin, and ampicillin were obtained from Shanghai Macklin Biochemical Technology Co., Ltd. (China). Cyanine 5.5 NHS ester (Cy5.5) was obtained from DuoFluor Inc. (Hubei, China). Tryptone and yeast extract were purchased from Oxoid Ltd. (China). *E. coli*, *AKK*, and *AKK*-corresponding bacterial culture medium were obtained from Beijing Beina Chuanglian Institute of Biotechnology (China).

Experimental apparatus

TEM images were carried out by JEOL JEM 2100F. Particle size was measured by a dynamic light scatterer (Malvern Zetasizer Nano ZS90). TGA was performed by Mettler TGA. Ultraviolet absorbance was measured by PerkinElmer VICTOR Nivo. In vivo imaging experiments were performed on IVIS imaging systems (PerkinElmer). Cell fluorescence was observed by inverted fluorescence microscopy (Olympus). Inductively coupled plasma mass spectrometry (ICP-MS) was measured by Agilent 7800.

Preparation of EGCG-coated liquid metal nano-agents

First, the LM nanoparticles were prepared according to our previous work (*36*). Briefly, LM (200 mg) was added into 15 ml of deoxidized ultrapure water (UPW) containing mPEG-SH (70 mg), and the mixture was ultrasonically treated with a 6-mmφ probe at 80% intensity for 40 min in an ice bath. Then, LM (200 mg) was added into 15 ml of deoxidized UPW containing EGCG (70 mg) or Cy5.5-labeled EGCG, and the mixture was ultrasonically treated with a 6-mmφ probe at 80% intensity for 40 min in an ice bath. The mixture was centrifuged at 1000 rpm for 10 min, and the supernatant was collected and followed with 8000 rpm for 10 min to obtain LM-EGCG. The nano-agents were washed with UPW three times and stored at 4°C for further use. For the thermal gravimetric analysis of LM-EGCG, the obtained LM and LM-EGCG (100 mg) nanoparticles were analyzed by a thermal gravimetric analyzer under nitrogen conditions after lyophilization, and the weight loss was recorded and analyzed.

Self-assembly of Ga^{3+} and EGCG in simulated colonic fluid

To explore the self-assembly behavior of Ga^{3+} and organic ligands, $Ga(NO_3)_3$ (2 mg ml^{-1}) was dropwise added into SCF containing EGCG, dopamine, sodium alginate, hyaluronic acid, trehalose anhydrous, or synanthrin (2 mg ml^{-1}), respectively. Next, the mixture was photographed at different time points (0.5, 1, 2, and 4 hours) and determined by a dynamic light scatterer to evaluate the generation of the Ga and EGCG complex. Afterward, we further assessed the self-assembly of Ga^{3+} and EGCG in SCF. First, $Ga(NO_3)_3$ (2 mg ml^{-1}) or EGCG (2 mg ml^{-1}) was separately added into SCF, and then another $Ga(NO_3)_3$ (2 mg ml^{-1}) solution was added into SCF containing EGCG (2 mg ml^{-1}). Then, the mixtures were photographed at different time points (0.5, 1, and 2 hours) and determined by a dynamic light scatterer.

RONS-scavenging ability of LM-EGCG

The ROS-scavenging capacity of LM-EGCG was tested by NBT. First, NBT, riboflavin, and methionine were severally dissolved in 0.05 M PBS to form 0.6 mg ml^{-1}, 49 mg ml^{-1}, and 3 μg ml^{-1} stock solutions. After that, 0.3 ml of reaction solution (PBS, EGCG, LM, or LM-EGCG, respectively) was added to 1.8 ml of PBS containing 0.3 ml of riboflavin, methionine, and NBT stock solutions. Then, the absorbance of the mixtures was measured at 560 nm after light irradiation for 20 min. Posteriorly, DPPH was applied to investigate the RNS-scavenging performance. Twenty microliters of reaction fluid (PBS, EGCG, LM, or LM-EGCG, respectively) was mixed with 180 μl of DPPH (0.12 mg ml^{-1}, soluble in methanol) and incubated for 3 to 30 min in the dark. Then, the absorbance of the mixture at 517 nm was measured by PerkinElmer VICTOR Nivo.

Intracellular RONS-scavenging capacity of LM-EGCG

The NCM460 and HUVEC cells were cultured in DMEM containing 10% FBS, penicillin (100 U ml^{-1}), and streptomycin (100 mg ml^{-1}) in a cell incubator at 37°C with 5% carbon dioxide. Intracellular ROS level was detected using DCFH-DA. First, 1×10^5 NCM460 cells were seeded in six-well plates and cultured for 24 hours, and then the culture medium was replaced by fresh DMEM containing LM, EGCG, or LM-EGCG (Ga concentration,

100 μg ml^{-1}). After incubation for 1 hour, the cells were treated with H_2O_2 (600 μM) for another 1 hour. The cells were observed in a fluorescence microscope after being stained with DCFH-DA for 30 min. Synchronously, DAF-FM DA was used to detect intracellular NO levels. HUVEC cells were incubated with LM, EGCG, or LM-EGCG (Ga concentration, 100 μg ml^{-1}) for 1 hour, respectively. Then, the cells were stained with DAF-FM DA after H_2O_2 incubation for 1 hour, followed by fluorescence microscope observation.

Animals

C57BL/6 mice (aged 6 to 8 weeks) with an average body weight of 20 g were purchased from Hubei Beiente Biotechnology Co., Ltd. All of the animal experiments were performed following the guidelines approved by the Institution Animal Care and Use Committee at Tongji Medical College (IACUC), Huazhong University of Science and Technology (Wuhan, China), and the corresponding IACUC number is 3501.

In vivo fluorescence imaging

For in vivo fluorescence imaging, first, the mice were fed with DSS in drinking water after being pre-treated with fluorescent-free feed for 1 week to build the IBD model. To investigate the augmented accumulation of LM-EGCG at the colonic site, IBD mice or healthy mice were treated with Cy5.5-labeled EGCG or LM-EGCG (Ga concentration, 5 mg kg^{-1}) by gavage. After 12 hours, the main organs including the heart, liver, spleen, lung, kidney, and gastrointestinal tissues for those mice, were collected for fluorescence imaging.

ICP-MS analysis of Ga^{3+} in mice

To investigate the enhancive accumulation of Ga in the inflamed site, DSS-treated mice or healthy C57BL/6 mice ($n = 3$) were orally administrated with $Ga(NO_3)_3$, LM, or LM-EGCG solution (Ga concentration, 5 mg kg^{-1}). After 12 hours, the mice were euthanized and the main organs (heart, liver, spleen, lung, and kidney), stomach, small intestine, and colon tissues were collected for the ICP-MS test to analyze the Ga^{3+} content. The colonic contents were collected for EDS elements imaging and EXAFS analysis. For the purpose of testing the state of LM-EGCG in the stomach and the potential excretion way from the urine, the stomach contents, blood, and urine in DSS-induced colitis mice were collected for ICP analysis after oral gavage of LM-EGCG at different time points.

LM-EGCG relieves DSS-induced IBD

C57BL/6 mice were acclimatized 1 week before random assignment to experimental groups ($n = 6$). The mice in the healthy group were treated with normal water only, while the other groups were fed with drinking water containing 2.5% (w/v) DSS for 8 days (days 0 to 7). Then, IBD mice were orally administered with PBS, 5-ASA (40 mg kg^{-1}), EGCG (5 mg kg^{-1}), $Ga(NO_3)_3$, LM, Ga-EGCG, or LM-EGCG (Ga concentration, 5 mg kg^{-1}) on days 5, 7, and 9, respectively. The body weight of all mice was recorded daily over the 10-day experiments. On day 10, fecal samples from those mice were collected for 16*S* rRNA analysis. Briefly, DNA was extracted and examined by 1% agarose gel electrophoresis. Extracted DNA was then rendered PCR (ABI GeneAmp 9700) which was specific to the V3 and V4 regions of the 16*S* rRNA gene and used to construct 16*S* rRNA libraries for community analysis by using TruSeqTM DNA Sample Prep Kit. The libraries were sequenced using the Mi-Seq Illumina sequencer. Meanwhile, all mice were euthanized on day 10, and the colonic tissues were collected for Bio-TEM imaging, immunofluorescence staining (ZO-1, occludin-1, occludin, iNOS, and Arg-1), H&E staining, and ELISA analysis. Colon tissues were homogenized in 1 ml of RIPA containing protease inhibitor, and then subjected to centrifugation at 5000*g* for 15 min at 4°C. Then, the supernatant was retained, and the concentration of protein was measured by BCA. Next, MPO, IL-6, TNF-α, IL-1β, IL-10, and TGF-β levels were determined by ELISA kit ($n = 5$).

Transcriptome sequencing analysis

The feces were collected for SCFAs detection by using gas chromatography–mass spectrometry at the end of treatment. Thereafter, the experimental mice were euthanized to collect the frozen colon sections for transcriptomic analysis. After successful extraction by the TRIZol method, RNA was dissolved by adding 50 μl of DEPC-treated water. Subsequently, total RNA was identified and quantified using a Qubit fluorescence quantifier and a Qsep400 high-throughput biofragment analyzer. After passing the library check, the different libraries were sequenced in Illumina after pooling them according to the effective concentration and the target sequencing output data volume, yielding 150–base pair paired-end reads. Four types of fluorescently labeled dNTPs, DNA polymerase, and junction primers were added to the sequencing flow cell for amplification. Data quality control was performed using fastp to remove reads with adapters. Paired-end reads were removed under the following conditions: when the number of N in any sequencing read exceeded 10% of the length of that read and when any sequencing read contained low-quality bases ($Q \leq 20$) exceeding 50% of the length of that read. Subsequent analyses were based on clean reads. DESeq2 was used for differential gene expression analysis between two groups, and Benjamini and Hochberg correction was applied to *P* values. Corrected *P* values and $\log_2$ fold change were used as thresholds for noteworthy differential expression. Enrichment analysis was performed on the basis of the hypergeometric test, with pathway-based hypergeometric distribution testing for KEGG and GO analysis.

Ga^{3+} influences bacterial proliferation

E. coli colonies were inoculated into centrifuge tubes (under a sterile environment) containing 10 ml of LB medium (10 g of tryptone, 5 g of yeast extract, 10 g of NaCl, and 1000 ml of water) and shaken at 37°C for 20 hours. *AKK* colonies were seeded in fluid thioglycollate medium under an oxygen-free environment and cultured at 37°C for 3 days. To investigate the influence of Ga^{3+} on bacteria, *E. coli* and *AKK* cultures were diluted to 1×10^4 CFU ml^{-1} and treated with various concentrations of $Ga(NO_3)_3$ (Ga concentration, 51, 64, 80, and 100 mg $liter^{-1}$, respectively). Bacteria were calculated by measuring the absorbance of suspension and the CFUs were quantified by the spread-plate method.

LM-EGCG alleviates antibiotics-pretreated IBD

Before feeding with DSS, C57BL/6 mice (aged 6 to 8 weeks) were pretreated with a cocktail of antibiotics (metronidazole, 1 g $liter^{-1}$; vancomycin, 0.5 g $liter^{-1}$; neomycin, 1 g $liter^{-1}$; and ampicillin, 1 g $liter^{-1}$) in drinking water for 5 days. Then, IBD mice were orally administered with PBS, EGCG (5 mg kg^{-1}), $Ga(NO_3)_3$, or LM-EGCG (Ga concentration, 5 mg kg^{-1}) on days 5, 7, and 9, respectively. On day 10, all mice were euthanized, and the main organs (liver, spleen, kidney, heart, and lung) were collected for H&E staining. Colonic tissues were collected for Bio-TEM imaging, immunofluorescence staining (ZO-1, occludin-1, occludin, iNOS, and Arg-1), H&E staining, and ELISA analysis.

Delayed treatment of IBD

After being fed with DSS for 11 days, the mice were orally administered with PBS, EGCG (5 mg kg^{-1}), $Ga(NO_3)_3$, or LM-EGCG (Ga concentration, 5 mg kg^{-1}) on days 10, 12, and 14, respectively. On day 15, all mice were euthanized, and the colonic tissues were collected for immunofluorescence staining (ZO-1, occludin-1, occludin, iNOS, and Arg-1), Bio-TEM imaging, H&E staining, and ELISA analysis.

Cytotoxicity evaluation of LM-EGCG

The cytotoxicity of LM-EGCG against NCM460 cells was evaluated by live/dead staining and MTT assay. First, 1×10^5 NCM460 cells were seeded in six-well plates for 24 hours and treated with $Ga(NO_3)_3$, Ga-EGCG, LM, or LM-EGCG (Ga concentration, 200, 400, and 800 μg ml^{-1}, respectively) for 24 hours. Then, the cells were observed by a fluorescence microscope after being stained with calcein-AM and PI. Meanwhile, an MTT assay was conducted to assess the cytotoxicity of LM-EGCG. A total of 5×10^3 NCM460 cells were seeded in 96-well plates and cultured for 24 hours. Then, cells were treated with $Ga(NO_3)_3$, EGCG, Ga-EGCG, or LM-EGCG and incubated for 24 hours. After MTT addition for 4 hours, the reagent was discarded, and 150 μl of DMSO was added to the 96-well plates. Last, the OD values of each well were measured at 570 nm on an enzyme standard. The cell viability calculation is as follows: $(OD_{samples} - OD_{DMSO})/(OD_{control} - OD_{DMSO}) \times 100\%$.

Safety assessment of LM-EGCG

The blood of healthy mice or IBD mice ($n = 4$) was collected after inflammatory therapy to detect the liver function index including ALT, TBIL, ALB, ALP, and TP and kidney function index containing Urea, Crea, and GLU variation. Besides, the red blood cells derived from healthy mice were used for hemolysis experiments. The red blood cells were treated with H_2O, PBS, $Ga(NO_3)_3$, LM, EGCG, Ga-EGCG, and LM-EGCG with different concentrations (Ga concentration, 100, 200, and 400 μg ml^{-1}, respectively). After incubation for 1 hour, the mixture was centrifuged (1000*g*, 3 min) to observe the color of the supernatant. To estimate the excretion of LM-EGCG in the digestive tract, healthy C57BL/6 mice ($n = 3$) were oral gavage of $Ga(NO_3)_3$, LM, or LM-EGCG (Ga concentration, 200 μg ml^{-1}), respectively, and the feces from those of mice was collected at different time points for ICP-MS analysis.

Statistical analysis

Statistical analysis was performed by Origin 9.0 or Prism 7.0 (GraphPad, USA). All data were presented as means ± SD. The results were analyzed with one-way or two-way analysis of variance (ANOVA) with the least significance difference test among the three groups. Differences were considered statistically significant if $P < 0.05$ ($^*P < 0.05$, $^{**}P < 0.01$, $^{***}P < 0.001$, and $^{****}P < 0.0001$).

Supplementary Materials

This PDF file includes:

Figs. S1 to S28

REFERENCES AND NOTES

1. D. R. Plichta, D. B. Graham, S. Subramanian, R. J. Xavier, Therapeutic opportunities in inflammatory bowel disease: Mechanistic dissection of host-microbiome relationships. *Cell* **178**, 1041–1056 (2019).
2. J. C. Clemente, J. Manasson, J. U. Scher, The role of the gut microbiome in systemic inflammatory disease. *BMJ* **360**, j5145 (2018).
3. M. Friedrich, M. Pohin, F. Powrie, Cytokine networks in the pathophysiology of inflammatory bowel disease. *Immunity* **50**, 992–1006 (2019).
4. Y. Lee, K. Sugihara, M. G. Gillilland, S. Jon, N. Kamada, J. J. Moon, Hyaluronic acid-bilirubin nanomedicine for targeted modulation of dysregulated intestinal barrier, microbiome and immune responses in colitis. *Nat. Mater.* **19**, 118–126 (2020).
5. A. D. Kostic, R. J. Xavier, D. Gevers, The microbiome in inflammatory bowel disease: Current status and the future ahead. *Gastroenterology* **146**, 1489–1499 (2014).
6. P. Praveschotinunt, A. M. Duraj-Thatte, I. Gelfat, F. Bahl, D. B. Chou, N. S. Joshi, Engineered *E. coli* Nissle 1917 for the delivery of matrix-tethered therapeutic domains to the gut. *Nat. Commun.* **10**, 5580 (2019).
7. Z. M. Geng, X. Y. Wang, F. Wu, Z. P. Cao, J. Y. Liu, Biointerface mineralization generates ultraresistant gut microbes as oral biotherapeutics. *Sci. Adv.* **9**, eade0997 (2023).
8. G. R. D'Haens, C. Jobin, Fecal microbial transplantation for diseases beyond recurrent clostridium difficile infection. *Gastroenterology* **157**, 624–636 (2019).
9. C. Zhang, H. Wang, X. H. Yang, Z. Fu, X. R. Ji, Y. F. Shi, J. Zhong, W. G. Hu, Y. Q. Ye, Z. T. Wang, D. L. Ni, Oral zero-valent-molybdenum nanodots for inflammatory bowel disease therapy. *Sci. Adv.* **8**, eabp9882 (2022).
10. W. H. Yang, D. M. Heithoff, P. V. Aziz, M. Sperandio, V. Nizet, M. J. Mahan, J. D. Marth, Recurrent infection progressively disables host protection against intestinal inflammation. *Science* **358**, 1588 (2017).
11. A. Alaarg, C. Pérez-Medina, J. M. Metselaar, M. Nahrendorf, Z. A. Fayada, G. Storm, W. J. M. Mulder, Applying nanomedicine in maladaptive inflammation and angiogenesis. *Adv. Drug Deliv. Rev.* **119**, 143–158 (2017).
12. S. Thorsteinsdottir, T. Gudjonsson, O. H. Nielsen, B. Vainer, J. B. Seidelin, Pathogenesis and biomarkers of carcinogenesis in ulcerative colitis. *Nat. Rev. Gastroenterol. Hepatol.* **8**, 395–404 (2011).
13. J. Liu, W. Li, Y. X. Wang, Y. Y. Ding, A. Lee, Q. Y. Hu, Biomaterials coating for on-demand bacteria delivery: Selective release, adhesion, and detachment. *Nano Today* **41**, 101291 (2021).
14. S. Zhao, Y. X. Li, Q. Y. Liu, S. R. Li, Y. Cheng, C. Q. Cheng, Z. Y. Sun, Y. Du, C. J. Butch, H. Wei, An orally administered CeO_2@montmorillonite nanozyme targets inflammation for inflammatory bowel disease therapy. *Adv. Funct. Mater.* **30**, 2004692 (2020).
15. J. K. Goodrich, E. R. Davenport, J. L. Waters, A. G. Clark, R. E. Ley, Cross-species comparisons of host genetic associations with the microbiome. *Science* **352**, 532–535 (2016).
16. B. R. Wilson, A. R. Bogdan, M. Miyazawa, K. Hashimoto, Y. Tsuji, Siderophores in iron metabolism: From mechanism to therapy potential. *Trends Mol. Med.* **22**, 1077–1090 (2016).
17. C. Ratledge, L. G. Dover, Iron metabolism in pathogenic bacteria. *Annu. Rev. Microbiol.* **54**, 881–941 (2000).
18. C. H. Goss, Y. Kaneko, L. Khuu, G. D. Anderson, S. Ravishankar, M. L. Aitken, N. Lechtzin, G. Zhou, D. M. Czyz, K. McLean, O. Olakanmi, H. A. Shuman, M. Teresi, E. Wilhelm, E. Caldwell, S. J. Salipante, D. B. Hornick, R. J. Siehnel, L. Becker, B. E. Britigan, P. K. Singh, Gallium disrupts bacterial iron metabolism and has therapeutic effects in mice and humans with lung infections. *Sci. Transl. Med.* **10**, eaat7520 (2018).
19. E. Mitidieri, D. Visaggio, E. Frangipani, C. Turnaturi, D. Vanacore, R. Provenzano, G. Costabile, R. Sorrentino, F. Ungaro, P. Visca, R. E. di Villa Bianca, Intra-tracheal administration increases gallium availability in lung: Implications for antibacterial chemotherapy. *Pharmacol. Res.* **170**, 105698 (2021).
20. A. Pandey, C. Savino, S. H. Ahn, Z. Y. Yang, S. G. V. Lanen, E. Boros, Theranostic gallium siderophore ciprofloxacin conjugate with broad spectrum antibiotic potency. *J. Med. Chem.* **62**, 9947–9960 (2019).
21. Y. C. Wang, B. J. Han, Y. X. Xie, H. B. Wang, R. M. Wang, W. Xia, H. Y. Li, H. Z. Sun, Combination of gallium(III) with acetate for combating antibiotic resistant *Pseudomonas aeruginosa*. *Chem. Sci.* **10**, 6099–6106 (2019).
22. A. B. Kelson, M. Carnevali, V. Truong-Le, Gallium-based anti-infectives: Targeting microbial iron-uptake mechanisms. *Curr. Opin. Pharmacol.* **13**, 707–716 (2013).
23. Y. Guo, W. M. Li, H. Y. Li, W. Xia, Identification and characterization of a metalloprotein involved in gallium internalization in *Pseudomonas aeruginosa*. *ACS Infect. Dis.* **5**, 1693–1697 (2019).
24. C. R. Chitambar, J. Narasimhan, Targeting iron-dependent DNA synthesis with gallium and transferrin-gallium. *Pathobiology* **59**, 3–10 (1991).
25. Y. Kaneko, M. Thoendel, O. Olakanmi, B. E. Britigan, P. K. Singh, The transition metal gallium disrupts Pseudomonas aeruginosa iron metabolism and has antimicrobial and antibiofilm activity. *J. Clin. Invest.* **177**, 887–888 (2007).
26. T. T. Xie, Y. C. Qi, Y. Y. Li, F. L. Zhang, W. L. Li, D. N. Zhong, Z. Tang, M. Zhou, Ultrasmall Ga-ICG nanoparticles based gallium ion/photodynamic synergistic therapy to eradicate biofilms and against drug-resistant bacterial liver abscess. *Bioact. Mater.* **6**, 3812–3823 (2021).
27. J. J. Yan, Y. Lu, G. J. Chen, M. Yang, Z. Gu, Advances in liquid metals for biomedical applications. *Chem. Soc. Rev.* **47**, 2518–2533 (2018).
28. W. J. Xie, F. M. Allioux, J. Z. Ou, E. Miyako, S. Y. Tang, Gallium-based liquid metal particles for therapeutics. *Trends Biotechnol.* **39**, 624–640 (2021).

29. N. L. Yang, F. Gong, Y. K. Zhou, Q. Yu, L. Cheng, Liquid metals: Preparation, surface engineering, and biomedical applications. *Coordin. Chem. Rev.* **471**, 214731 (2022).
30. J. J. Yan, M. H. Malakooti, Z. Lu, Z. Y. Wang, N. Kazem, C. F. Pan, M. R. Bockstaller, C. Majidi, K. Matyjaszewski, Solution processable liquid metal nanodroplets by surface-initiated atom transfer radical polymerization. *Nat. Nanotechnol.* **14**, 684–690 (2019).
31. J. Shu, D. A. Ge, E. L. Wang, H. T. Ren, T. Cole, S. Y. Tang, X. P. Li, X. B. Zhou, R. J. Li, H. Jin, W. H. Li, M. D. Dickey, S. W. Zhang, A liquid metal artificial muscle. *Adv. Mater.* **33**, e2103062 (2021).
32. X. L. Wang, L. L. Fan, J. Zhang, X. Y. Sun, H. Chang, B. Yuan, R. Guo, M. H. Duan, J. Liu, Printed conformable liquid metal e-skin-enabled spatiotemporally controlled bioelectromagnetics for wireless multisite tumor therapy. *Adv. Funct. Mater.* **29**, 1907063 (2019).
33. N. L. Yang, W. Li, F. Gong, L. Cheng, Z. L. Dong, S. Bai, Z. S. Xiao, C. F. Ni, Z. Liu, Injectable nonmagnetic liquid metal for Eddy-thermal ablation of tumors under alternating magnetic field. *Small Methods* **4**, 2000147 (2020).
34. J. J. Hu, M. D. Liu, Y. Chen, F. Gao, S. Y. Peng, B. R. Xie, C. X. Li, X. Zeng, X. Z. Zhang, Immobilized liquid metal nanoparticles with improved stability and photothermal performance for combinational therapy of tumor. *Biomaterials* **207**, 76–88 (2019).
35. S. A. Chechetka, Y. Yu, X. Zhen, M. Pramanik, K. Y. Pu, E. Miyako, Light-driven liquid metal nanotransformers for biomedical theranostics. *Nat. Commun.* **8**, 15432 (2017).
36. M. D. Liu, D. K. Guo, R. Y. Zeng, J. J. Ye, S. B. Wang, C. X. Li, Y. X. Sun, S. X. Cheng, X. Z. Zhang, Yolk-shell structured nanoflowers induced intracellular oxidative/thermal stress damage for cancer treatment. *Adv. Funct. Mater.* **30**, 2006098 (2020).
37. A. Elbourne, S. Cheeseman, P. Atkin, N. P. Truong, N. Syed, A. Zavabeti, M. Mohiuddin, D. Esrafilzadeh, D. Cozzolino, C. F. McConville, M. D. Dickey, R. J. Crawford, K. Kalantar-Zadeh, J. Chapman, T. Daeneke, V. K. Truong, Antibacterial liquid metals: Biofilm treatment via magnetic activation. *ACS Nano* **14**, 802–817 (2020).
38. K. Y. Kwon, S. Cheeseman, A. Frias-De-Diego, H. Hong, J. Y. Yang, W. Jung, H. Yin, B. J. Murdoch, F. Scholle, N. Crook, E. Crisci, M. D. Dickey, V. K. Truong, T. Kim, A liquid metal mediated metallic coating for antimicrobial and antiviral fabrics. *Adv. Mater.* **33**, e2104298 (2021).
39. Y. Xu, R. Rothe, D. Voigt, S. Hauser, M. Y. Cui, T. Miyagawa, M. P. Gaillez, T. Kurth, M. Bornhäuser, J. Pietzsch, Y. X. Zhang, Convergent synthesis of diversified reversible network leads to liquid metal-containing conductive hydrogel adhesives. *Nat. Commun.* **12**, 2407 (2021).
40. Y. L. Lin, X. Gao, J. P. Yue, Y. Fang, J. Y. Shi, L. Y. Meng, C. Clayton, X. X. Zhang, F. Y. Shi, J. J. Deng, S. Chen, Y. Jiang, F. Marin, J. T. Hu, H. M. Tsai, Q. Tu, E. W. Roth, R. Bleher, X. Q. Chen, P. Griffin, Z. H. Cai, A. Prominski, T. W. Odom, B. Tian, A soil-inspired dynamically responsive chemical system for microbial modulation. *Nat. Chem.* **15**, 119–128 (2023).
41. Z. H. Lin, C. Y. Gao, D. L. Wang, Q. He, Bubble-propelled janus gallium/zinc micromotors for the active treatment of bacterial infections. *Angew. Chem. Int. Ed.* **60**, 8750–8754 (2021).
42. B. N. Singh, S. Shankar, R. K. Srivastava, Green tea catechin, epigallocatechin-3-gallate (EGCG): Mechanisms, perspectives and clinical applications. *Biochem. Pharmacol.* **82**, 1807–1821 (2011).
43. B. Hu, S. J. Yu, C. Shi, J. Gu, Y. Shao, Q. Chen, Y. Q. Li, R. Mezzenga, Amyloid-polyphenol hybrid nanofilaments mitigate colitis and regulate gut microbial dysbiosis. *ACS Nano* **14**, 2760–2776 (2020).
44. J. J. Zhou, Z. X. Lin, Y. Ju, M. A. Rahim, J. J. Richardson, F. Caruso, Polyphenol-mediated assembly for particle engineering. *Acc. Chem. Res.* **53**, 1269–1278 (2020).
45. Z. M. Zhao, D. C. Pan, Q. M. Qi, J. Kim, N. Kapate, T. Sun, C. W. Shields IV, L. L. W. Wang, D. Wu, C. J. Kwon, W. He, J. L. Guo, S. Mitragotri, Engineering of living cells with polyphenol-functionalized biologically active nanocomplexes. *Adv. Mater.* **32**, e2003492 (2020).
46. H. Miyoshi, R. Ajima, C. T. Luo, T. P. Yamaguchi, T. S. Stappenbeck, Wnt5a potentiates TGF-β signaling to promote colonic crypt regeneration after tissue injury. *Science* **338**, 108–113 (2012).
47. K. A. Kles, E. B. Chang, Short-chain fatty acids impact on intestinal adaptation, inflammation, carcinoma, and failure. *Gastroenterology* **130**, S100–S105 (2006).
48. Z. L. Zhang, H. Zhang, T. Chen, L. Shi, D. R. Wang, D. Tang, Regulatory role of short-chain fatty acids in inflammatory bowel disease. *Cell Commun. Signal* **20**, 64 (2022).
49. J. Zhou, M. Y. Li, Q. F. Chen, X. J. Li, L. F. Chen, Z. L. Dong, W. J. Zhu, Y. Yang, Z. Liu, Q. Chen, Programmable probiotics modulate inflammation and gut microbiota for inflammatory bowel disease treatment after effective oral delivery. *Nat. Commun.* **1**, 3432 (2022).
50. Y. Lu, Q. Y. Hu, Y. L. Lin, D. B. Pacardo, C. Wang, W. J. Sun, F. S. Ligler, M. D. Dickey, Z. Gu, Transformable liquid-metal nanomedicine. *Nat. Commun.* **6**, 10066 (2015).
51. K. Yang, J. M. Wan, S. A. Zhang, Y. J. Zhang, S. T. Lee, Z. Liu, In vivo pharmacokinetics, long-term biodistribution, and toxicology of pegylated graphene in mice. *ACS Nano* **5**, 516–522 (2011).
52. H. J. Galipeau, E. F. Verdu, Protection from inflammatory bowel disease. *Science* **381**, 1153–1154 (2023).
53. J. G. Fox, T. C. Wang, Inflammation, atrophy, and gastric cancer. *J. Clin. Invest.* **117**, 60–69 (2007).
54. C. Q. Cheng, S. Zhao, Y. Cheng, Y. F. Liu, H. Wei, Design of nanozymes for inflammatory bowel disease therapy. *Sci. China Life Sci.* **64**, 1368–1371 (2021).
55. F. Cao, L. Jin, Y. Gao, Y. Ding, H. Wen, Z. Qian, C. Zhang, L. Hong, H. Yang, J. Zhang, Z. Tong, W. Wang, X. Chen, Z. Mao, Artificial-enzymes-armed *Bifidobacterium longum* probiotics for alleviating intestinal inflammation and microbiota dysbiosis. *Nat. Nanotechnol.* **18**, 617–627 (2023).
56. J. L. Yang, G. Z. Zhang, M. Y. Peng, S. C. Tan, S. C. Ge, Y. Xi, Y. Yang, Z. Y. Liang, L. Wen, T. H. Xie, S. X. W. Zhou, J. Y. An, Y. F. Wang, W. Liu, K. X. Zhang, Z. Z. Zhang, J. J. Liu, J. J. Shi, Bionic regulators break the ecological niche of pathogenic bacteria for modulating dysregulated microbiome in colitis. *Adv. Mater.* **34**, e2204650 (2022).
57. S. E. Winter, M. G. Winter, M. N. Xavier, P. Thiennimitr, V. Poon, A. M. Keestra, R. C. Laughlin, G. Gomez, J. Wu, S. D. Lawhon, I. E. Popova, S. J. Parikh, L. G. Adams, R. M. Tsolis, V. J. Stewart, A. J. Baumler, Host-derived nitrate boosts growth of *E. coli* in the inflamed gut. *Science* **339**, 708–711 (2013).
58. O. Hartwig, M. A. S. Boushehri, K. S. Shalaby, B. Loretz, A. Lamprecht, C. M. Lehr, Drug delivery to the inflamed intestinal mucosa-targeting technologies and human cell culture models for better therapies of IBD. *Adv. Drug Deliver. Rev.* **175**, 113828 (2021).
59. S. F. Zhanga, R. Langera, G. Traversoa, Nanoparticulate drug delivery systems targeting inflammation for treatment of inflammatory bowel disease. *Nano Today* **16**, 82–96 (2017).
60. Q. X. Huang, J. L. Liang, C. H. Yang, K. Li, M. T. Niu, J. X. Fan, X. Z. Zhang, Stimulation-responsive mucoadhesive probiotics for inflammatory bowel disease treatment by scavenging reactive oxygen species and regulating gut microbiota. *Biomaterials* **301**, 122274 (2023).
61. J. Liu, Y. X. Wang, W. J. Heelan, Y. Chen, Z. T. Li, Q. Y. Hu, Mucoadhesive probiotic backpacks with ROS nanoscavengers enhance the bacteriotherapy for inflammatory bowel diseases. *Sci. Adv.* **8**, eabp8798 (2022).
62. M. Schirmer, A. Garner, H. Vlamakis, R. J. Xavier, Microbial genes and pathways in inflammatory bowel disease. *Nat. Rev. Microbiol.* **17**, 497–511 (2019).
63. X. Y. Yang, J. L. Yang, Z. H. Ye, G. Z. Zhang, W. M. Nie, H. Cheng, M. Y. Peng, K. X. Zhang, J. J. Liu, Z. Z. Zhang, J. J. Shi, Physiologically inspired mucin coated *Escherichia coli* Nissle 1917 enhances biotherapy by regulating the pathological microenvironment to improve intestinal colonization. *ACS Nano* **16**, 4041–4058 (2022).
64. W. Zhu, M. G. Winter, M. X. Byndloss, L. Spiga, B. A. Duerkop, E. R. Hughes, L. Buttner, E. de Lima Romao, C. L. Behrendt, C. A. Lopez, L. Sifuentes-Dominguez, K. Huff-Hardy, R. P. Wilson, C. C. Gillis, C. Tukel, A. Y. Koh, E. Burstein, L. V. Hooper, A. J. Baumler, S. E. Winter, Precision editing of the gut microbiota ameliorates colitis. *Nature* **553**, 208–211 (2018).
65. A. V. Vila, F. Imhann, V. Collij, S. A. Jankipersadsing, T. Gurry, Z. Mujagic, A. Kurilshikov, M. J. Bonder, X. F. Jiang, E. F. Tigchelaar, J. Dekens, V. Peters, M. D. Voskuil, M. C. Visschedijk, H. M. Dullemen, D. Keszthelyi, M. A. Swertz, L. Franke, R. Alberts, E. A. M. Festen, G. Dijkstra, A. A. M. Masclee, M. H. Hofker, R. J. Xavier, E. J. Alm, J. Y. Fu, C. Wijmenga, D. M. A. E. Jonkers, A. Zhernakova, R. K. Weersma, Gut microbiota composition and functional changes in inflammatory bowel disease and irritable bowel syndrome. *Sci. Transl. Med.* **10**, eaap8914 (2018).
66. T. Lee, T. Clavel, K. Smirnov, A. Schmidt, I. Lagkouvardos, A. Walker, M. Lucio, B. Michalke, P. Schmitt-Kopplin, R. Fedorak, D. Haller, Oral versus intravenous iron replacement therapy distinctly alters the gut microbiota and metabolome in patients with IBD. *Gut* **66**, 863–871 (2017).

Acknowledgments: This work was supported by the Integrated Innovative Team for Major Human Diseases Program of Tongji Medical College, HUST, and the Academic Doctor Supporting Program of Tongji Medical College, HUST. **Funding:** This work was supported by the National Key Research and Development Program of China (2022YFC2408100) to L.W., the National Natural Science Foundation Program of China (82272277) to L.W., the National Natural Science Foundation Program of China (82072167) to L.W., the National Natural Science Foundation Program of China (81974382) to Z.W., the National Natural Science Foundation Program of China (82173315) to Z.W., and the Major Scientific and Technological Innovation Projects of Hubei Province (2022BCA013) to Z.W. **Author contributions:** Conceptualization: M.L., J.Z., H.L., Y.Z., L.W., and Z.W. Methodology: M.L., J.Z., H.L., Y.Z., and Q.C. Project ministration: M.L., J.Z., H.L., Y.Z., L.W., and Z.W. Resources: M.L., J.Z., H.L., Y.Z., J.L., and Q.L. Investigation: M.L., J.Z., H.L., Y.Z., and L.W. Visualization: M.L., J.Z., H.L., Y.Z., Q.L., Q.C., and Z.W. Validation: M.L., J.Z., H.L., Y.Z., Q.L., and Z.W. Data curation: M.L., J.Z., H.L., and Y.Z. Software: M.L., J.Z., H.L., and Y.Z. Formal analysis: M.L., J.Z., H.L., Y.Z., Q.C., and Q.L. Supervision: M.L., J.Z., H.L., Z.W., and L.W. Funding acquisition: Z.W. and L.W. Writing—original draft: M.L., J.Z., H.L., Y.Z., Q.C., and Z.W. Writing—review and editing: M.L., J.Z., H.L., Y.Z., Q.C., J.L., Q.L., Z.W., and L.W. **Competing interests:** The authors declare that they have no competing interests. **Data and materials availability:** All data needed to evaluate the conclusions in the paper are present in the paper and/or the Supplementary Materials.

Submitted 28 November 2023
Accepted 6 June 2024
Published 12 July 2024
10.1126/sciadv.adn1745